HHS Public Access

Author manuscript

Cell. Author manuscript; available in PMC 2018 February 23.

Published in final edited form as:

Cell. 2017 February 23; 168(5): 878–889.e29. doi:10.1016/j.cell.2017.02.006.

Multivalent small molecule pan-RAS inhibitors

Matthew E. Welsch[1], **Anna Kaplan**[2], **Jennifer M. Chambers**[2], **Michael E. Stokes**[2], **Pieter H. Bos**[2], **Arie Zask**[2], **Yan Zhang**[1], **Marta Sanchez-Martin**[3], **Michael A. Badgley**[4,5], **Christine S. Huang**[2], **Timothy H. Tran**[2], **Hemanth Akkiraju**[2,6], **Lewis M. Brown**[2,6], **Renu Nandakumar**[7], **Serge Cremers**[4,7], **Wan S. Yang**[8], **Liang Tong**[2], **Kenneth P. Olive**[4,5], **Adolfo Ferrando**[3,4,9], and **Brent R. Stockwell**[1,2,10,*]

[1]Department of Chemistry, Columbia University, New York, NY 10027

[2]Department of Biological Sciences, Columbia University, New York, NY

[3]Institute for Cancer Genetics, Columbia University Medical Center, New York, NY

[4]Department of Pathology, Columbia University Medical Center, New York, NY

[5]Division of Digestive and Liver Diseases in the Department of Medicine, Columbia University Medical Center, New York, NY

[6]Quantitative Proteomics and Metabolomics Center, Columbia University, New York, NY

[7]Irving Institute for Clinical and Translational Research, Columbia University Medical Center, New York, NY

[8]Department of Biological Sciences, St. John's University, Queens, NY 11439

[9]Department of Pediatrics, Columbia University Medical Center, New York, NY

SUMMARY

Design of small molecules that disrupt protein-protein interactions, including the interaction of RAS proteins and their effectors, have potential use as chemical probes and therapeutic agents. We describe here the synthesis and testing of potential small molecule pan-RAS ligands, which were designed to interact with adjacent sites on the surface of oncogenic KRAS. One compound, termed 3144, was found to bind to RAS proteins using microscale thermophoresis, nuclear magnetic

*Correspondence to: bstockwell@columbia.edu.

[10]Lead Contact

Author Contributions

M.E.W., B.R.S. and J.M.C. designed, performed and analyzed the results of computational analyses and synthetic chemistry. A.K. and B.R.S. designed, performed and analyzed the results of molecular cloning, protein expression, purification, ITC, and protein NMR analyses. M.E.W., A.K., J.M.C. and B.R.S. designed, performed and analyzed MST experiments. A.K., C.H., T.T. and L.T. generated x-ray crystal structures. M.E.S., Y.Z., M.E.W. and B.R.S. designed, performed and analyzed cell culture studies. M.S.-M. and A.F. performed and analyzed in vitro and in vivo studies with T-ALL patient samples. P.B., A.Z. and B.R.S. designed, performed and analyzed cell accumulation and metabolic stability in liver microsomes. M.E.W., W.S.Y., and B.R.S. designed, performed and analyzed the cell-line xenograft study. M.A.B., M.E.W., B.R.S. and K.P.O. designed, performed and analyzed the KPC mouse study. J.M.C., B.R.S., R.N. and S.C. designed, performed and analyzed in vivo pharmacokinetics. B.R.S. supervised the overall project. B.R.S. and M.E.W. wrote the manuscript, with input from other authors.

resonance spectroscopy and isothermal titration calorimetry, and to exhibit lethality in cells partially dependent on expression of RAS proteins. This compound was metabolically stable in liver microsomes and displayed anti-tumor activity in xenograft mouse cancer models. These findings suggest that pan-RAS inhibition may be an effective therapeutic strategy for some cancers, and that structure-based design of small molecules targeting multiple adjacent sites to create multivalent inhibitors may be effective for some proteins.

Keywords

Ras; Kras; Nras; Hras; cancer; small molecule; drug design; chemical biology; GTPase; multivalent

INTRODUCTION

Small molecule drugs act by binding to proteins; those proteins that harbor sites amenable to small molecule binding are termed druggable (Hopkins and Groom, 2002). An important class of proteins that is challenging from the standpoint of small molecule ligand discovery consists of proteins that exert biological effects through protein-protein interactions (Arkin et al., 2014; Arkin and Wells, 2004). While some protein-protein interactions consisting of short alpha helical domains inserted into a hydrophobic pocket in an interacting protein have been amenable to disruption with small molecules (*e.g.,* the p53-Mdm2 interaction (Vassilev et al., 2004)), most protein-protein interactions have been challenging to inhibit with small molecules. Within this category of challenging targets is the RAS family of GTPases. Despite numerous efforts to target these oncogenic proteins, therapeutic agents that directly inhibit the oncogenic effects of RAS proteins have been challenging to create (Cox et al., 2014); this is noteworthy because RAS proteins have been extensively studied due to their high prevalence and frequent essentiality in lethal malignancies (Downward, 2003).

Mutations RAS genes are commonly found in numerous malignancies, including pancreatic (90%), colon (45%), and lung cancers (35%) (Prior et al., 2012). Many tumor types have been shown to be dependent on continued expression of oncogenic RAS proteins in cell and animal models (McCormick, 2011). The critical ongoing role of RAS proteins in the viability, maintenance and growth of many cancers, and the inability of researchers to develop drugs directly targeting RAS proteins has motivated alternative approaches, such as synthetic lethal screening; to date, however, this approach has not yielded promising drug candidates for RAS mutant cancers (Dolma et al., 2003; Kaelin, 2005; Yang and Stockwell, 2008).

The RAS proteins function in signal transduction pathways controlling cell growth and differentiation as binary switches, transitioning from an inactive GDP-bound state to an active GTP-bound state (Karnoub and Weinberg, 2008; Malumbres and Barbacid, 2003; Prior and Hancock, 2012). GTP binding enables several residues, primarily in the switch I region (residues 30–40) and the switch II region (residues 60–70) to adopt a conformation that permits RAS effector proteins to bind; this switch is regulated by GTPase activating proteins (GAPs) and guanine nucleotide exchange factors (GEFs) (Hall et al., 2002). Mutations that result in the impairment of the intrinsic GTPase activity of RAS proteins, or

that prevent GAP binding, activate downstream signaling pathways and contribute to tumor formation and maintenance (Block et al., 1996; Huang et al., 1998; Huang et al., 1997; Pacold et al., 2000).

RAS proteins have been challenging drug targets, primarily due to the lack of a sufficiently large and deep hydrophobic pocket for small molecule binding, aside from the challenging nucleotide-binding site (Cox et al., 2014; Gysin et al., 2011; Shima et al., 2013; Spiegel et al., 2014; Stephen et al., 2014; Sun et al., 2012; Wang et al., 2012). Previous efforts, which have included fragment-based experimental screening, have focused on identifying and targeting individual shallow sites on RAS proteins, (Burns et al., 2014; Cox et al., 2014; Maurer et al., 2012; Ostrem et al., 2013; Shima et al., 2013; Sun et al., 2012; Sun et al., 2014). Targeting such sites has yet to yield ligands with sufficient potency and selectivity to enable *in vivo* exploration of contexts in which RAS proteins serve as viable pharmacological targets. This observation motivated our hypothesis that instead of targeting a single site on RAS proteins, we might be able to design ligands that target multiple sites, enabling sufficient affinity and selectivity for pharmacological RAS inhibition. Moreover, given frequent addiction to mutated RAS proteins, we hypothesized that pan-RAS inhibition (*i.e.*, simultaneous inhibition of the products of the *HRAS*, *NRAS* and *KRAS* genes) would be therapeutically beneficial, despite the essentiality of *Kras* for normal mouse development (Johnson et al., 1997). Here, we report the design and testing of candidate small molecule pan-RAS inhibitors; these compounds were designed to prevent effector protein binding; we focused on one compound that was found to bind to RAS proteins *in vitro*, and to cause inhibition of tumor growth in animal models of RAS-dependent cancers. This approach represents a potential therapeutic strategy for treating RAS-dependent cancers and demonstrates that structure-based computational design of small molecules targeting two or more sites may be effective for otherwise challenging drug targets.

RESULTS

Our initial efforts focused on analyzing the interaction of $KRAS^{G12D}$ with effector proteins and attempting to identify small molecule binding sites that are also functionally relevant. We noted that mutagenesis of the residues in a stretch of amino acids in the switch I region (Figure 1A) (*i.e.*, I36 - S39), or of the interacting residues on the primary effector proteins (RAF, PI3K or RALGDS), has been reported to lower binding affinity for effector proteins to RAS proteins (Colicelli, 2004; Gysin et al., 2011; Hall et al., 2002; Huang et al., 1998; Huang et al., 1997; Karnoub and Weinberg, 2008; Malumbres and Barbacid, 2003; Pacold et al., 2000; Scheffzek et al., 1997; Shaw and Cantley, 2006; Tanaka and Rabbitts, 2010; Tsutsumi et al., 2009; Vigil et al., 2010; Walker and Olson, 2005). Analysis of the $KRAS^{G12D}$ (PDB: 4DSN, and see Supporting Information) structure revealed a candidate site in the switch I region (termed here the D38 site), and two additional potential binding sites near the D38 site (Figure 1B and Supporting Information): we identified a site centered on alanine 59 (termed the A59 site), located between the switch I and switch II regions; on the other side of the D38 site, we identified a potential binding site near Y32 (Figure 1B and Supporting Information).

We computationally docked (using Glide SP, Schrödinger Inc.) designed fragment-like and lead-like small molecules into each of these sites on $KRAS^{G12D}$. Small molecule libraries were designed spanning two or three of these sites, with the goal of generating compounds with improved affinity and specificity. Among the top-ranked fragments selected for the D38 site, we observed a substantial number of aliphatic rings that contained protonated amines making electrostatic interactions with the carboxylic acid functional groups of D38 and D33. In the adjacent A59 site, several of the top-scoring fragments contained an indole. We calculated the predicted physiochemical properties (using Qikprop, Schrödinger Inc) of the most promising compounds, to determine if they would be ultimately suitable for *in vivo* testing, given the larger molecular weights required for creating favorable predicted interactions with two or more sites. While the molecular weights surpassed the ideal range for orally bioavailable molecules (*e.g.*, Figure 1C and Figure S1C) and predicted logP values were larger than is typically seen for orally available drugs, other properties were potentially suitable (Figure S1A, C). After synthesizing and testing a number of candidate compounds (see Supporting Information), we focused on compound 3144 as the most promising candidate inhibitor (see Supporting Information for a list of compounds synthesized and tested). Compound 3144 (Figure 1C, S1A) was docked into the analogous site on other small GTPases in the RAS superfamily, which yielded less favorable docking scores, suggesting potential RAS protein selectivity (Figure S1B).

The small molecule 3144 binds to $KRAS^{G12D}$ in MST, ITC and NMR assays

We observed that the ^{19}F NMR spectrum of 10 μM 3144, which bears a trifluoromethoxy group, contained a single peak, as expected (Figure 2A); addition of 20 μM $KRAS^{G12D}$ bound to the non-hydrolyzable GTP analog GppNHp (see Supporting Information) to 3144 resulted in loss of this ^{19}F peak, presumably due to protein binding (Figure 2A), suggesting a K_D for the 3144-$KRAS^{G12D}$-GppNHp interaction of < 20 μM. Increasing the concentration of compound 3144 resulted in the reappearance of a single peak in the ^{19}F spectrum, presumably due to unbound excess ligand (Figure 2A). These data suggest that compound 3144 binds to $KRAS^{G12D}$-GppNHp with an affinity less than 20 μM under these conditions.

To further validate and characterize the interaction between 3144 and $KRAS^{G12D}$, we measured the interaction using isothermal titration calorimetry (ITC) and HSQC NMR (Figure 2B and Figure S2). Calorimetric titration of $KRAS^{G12D}$-GppNHp into a solution of compound 3144 showed exothermic binding with dissociation constant (K_D) of 17.8 ± 4.5 μM, consistent with the ^{19}F NMR assay data (Figure 2B). In addition, the ^{1}H-^{15}N HSQC spectrum (Figure S2A, B) showed changes in amide resonances were observed in residues S39, D38, E37 and I36, consistent with the predicted docking pose (Figure S2C).

We used another independent biophysical method to test binding of 3144 to $KRAS^{G12D}$: we performed microscale thermophoresis (MST) using labeled GppNHp-loaded $KRAS^{G12D}$. We measured a dissociation constant of 9 μM +/−1 μM for the interaction between 3144 and $KRAS^{G12D}$-GppNHp using MST (Figure 2C). Consistent with modeling and docking (Figure S1), we detected a reduced affinity of 3144 for the GDP complex of $KRAS^{G12D}$ (Figure 2C).

To verify the nature of the nucleotide bound to the protein used in these assays, we evaluated the composition to $KRAS^{G12D}$ in each sample (see Supporting Information). We found that exchange of the endogenous nucleotide that is normally retained after protein purification caused a reliable shift in the melting temperature of the $KRAS^{G12D}$ protein, allowing us to measure the efficiency of nucleotide exchange (Figure 2F). Nucleotide exchange was then confirmed directly by mass spectrometry: protein preparations were diluted into a denaturing buffer (50% MeOH with 0.05% formic acid) or into a native mode buffer (10 mM ammonium acetate), and each protein solution analyzed by mass spectrometry (see Supporting Information). The nucleotide-free apoprotein ($KRAS^{G12D}$) was the predominant species in the denaturing buffer methanol, but was not detected in ammonium acetate, suggesting that ammonium acetate was effective in retaining the native structure of the protein (Figure S2E). For spectra recorded in ammonium acetate, purified protein appeared as a mixture bound to GDP and GTP nucleotides, as expected. In addition, this exchange protocol was effective for both GDP and GTP (Figure S2F): no GTP was detected in the GDP-exchanged samples, and no GDP was detected in the GTP-exchanged samples. In contrast, GppNHp exchange resulted in a mixture of $KRAS^{G12D}$ containing either GppNHp or GDP, likely due to the lower affinity of RAS proteins for this non-hydrolyzable nucleotide analog (Figure S2E). Thus, these preparations of $KRAS^{G12D}$-GTP and $KRAS^{G12D}$-GDP were pure with the expected nucleotide present, and the preparation of $KRAS^{G12D}$-GppNHp was a mixture of $KRAS^{G12D}$ bound to GDP and GppNHp. The presence of contaminating GDP nucleotide in the $KRAS^{G12D}$-GppNHp samples may account for the modest shift in affinity of 3144 in comparing GppNHp-bound protein and GDP-bound protein in this assay (Figure 2C). It is notable that some compounds designed to bind to three sites had improved affinity, but at the expense of a larger molecular weight, lower aqueous solubility and possibly less favor physicochemical properties (Figure 2C); therefore we continued to focus our studies on compound 3144 to evaluate the feasibility of targeting two adjacent sites on RAS proteins to generate pan-RAS inhibitors.

To test whether the compound 3144 bound to $KRAS^{G12D}$ in the predicted binding site, we generated two point mutants (D38A and I36N) that were predicted to reduce the binding affinity of 3144, and found that these mutant proteins displayed reduced binding affinity of 3144 in the MST assay (Figure 2C). We confirmed that these mutant proteins could also be exchanged with GTP, and so were still capable of binding nucleotide in a manner similar to $KRAS^{G12D}$ (Figure 2E, F).

To assess target selectivity, we measured binding of compound 3144 to other RAS superfamily small GTPases using MST. We detected binding to $KRAS^{G12D}$, $KRAS^{wt}$, $HRAS^{wt}$ and $NRAS^{wt}$, but not to other small GTPases in the RAS superfamily, with the exception of RRAS2, which showed weak binding (Figure 2D).

We attempted to obtain a crystal structure of compound 3144 bound to $KRAS^{G12D}$ or $KRAS^{G12V}$: 960 different crystallization conditions were screened with these proteins at 70 mg/ml and 20 mg/ml concentrations. The higher concentration yielded crystal structures of $KRAS^{G12D}$ Mg-GDP and Mg-GppNHp complexes at up to 1.83 Å resolution, which were nearly identical to published structures (Figure S2D and Supporting Information) (Ostrem and Shokat, 2016). We were also able to obtain a crystal structure of $KRAS^{G12V}$ in complex

with Mg-GDP (Figure S2D and Supporting Information). By comparing the G12V and G12D KRAS structures, we determined that 3144 should bind with similar affinity to both mutants, as they are essentially identical. Co-crystallization experiments with a stoichiometric amount of 3144 were not successful at yielding a ligand-bound structure, possibly due to limited solubility. Our attempts at using sub-stoichiometric concentrations for co-crystallization and crystal soaking did not yield any structures of the 3144-protein complex.

Activity of 3144 in cell lines

We next sought to test whether compound 3144 had RAS inhibitory activity in a cellular context. Given that this compound was capable of binding to HRAS, KRAS and NRAS in the MST assay, we evaluated whether combined knockdown of *KRAS*, *NRAS* and *HRAS* genes (Supplemental Table S2) would sensitize cancer cells to 3144; to test this, we identified a less RAS-addicted cell line (DLD-1, with $KRAS^{G13D}$) in which pan-RAS knockdown was not on its own substantially lethal at high cell densities (Figure 3A, S3AB). We found that while DLD-1 cells were resistant to 3144 up to 20 μM under these conditions, combined knockdown of *HRAS*, *NRAS* and *KRAS* resulted in sensitization to 3144 lethality, as expected for a pan-RAS inhibitor (Figure 3A). Pan-RAS knockdown did not sensitize DLD-1 cells to the lethality of MG132, a proteasome inhibitor, indicating that the sensitization to 3144 is not a general sensitization to lethal compounds (Figure 3A, Figure S3AB).

To further examine the potential RAS-dependent lethality of 3144, we used a previously reported mouse embryo fibroblast (MEF) cell line in which murine *Hras* and *Nras* had been deleted, and only *Kras* remained, flanked by loxP sites; a tamoxifen-inducible Cre recombinase was also expressed in these $Kras^{lox/lox}$, $Hras^{-/-}$, $Nras^{-/-}$ $RERTn^{ert/ert}$ cells (Urosevic et al., 2009). We found that these cells were sensitive to the lethality of compound 3144, as expected (IC_{50} = 3.8 μM, Figure 3B); however, excision of *Kras* from these cells using tamoxifen, and introduction of membrane-targeted $BRAF^{V600E}$-CAAX resulted in resistance to 3144 (Figure 3B), indicating a degree of *Kras*-dependent lethality. The lethality of 3144 in $BRAF^{V600E}$-CAAX-expressing MEF cells at concentrations of 20 μM and above may reflect residual expression of *Kras* due to incomplete excision, or off-target lethality of 3144, perhaps including RRAS2 inhibition (Figure S4). The sensitivity of these lines to vemurafenib, a $BRAF^{V600E}$ inhibitor, was reversed, as expected, with $BRAF^{V600E}$-CAAX-expressing cells being more sensitive, indicating the resistance caused by $BRAF^{V600E}$-CAAX expression did not cause a general resistance to lethal compounds (Figure 3B). Moreover, we found that at concentrations below 3 μM, 3144 did not reduce the number of MEFs below the starting number (Figure S4A–C); given that treatment of these cells with 4-OHT does not result in complete lethality, but rather arrest (Figure 4B), this suggested that at some concentrations, 3144 is cytostatic, possibly due to pan-RAS inhibition.

We also tested the lethality of 3144 in a panel of 11 cancer cell lines with different RAS isoform mutations and various degrees of RAS dependency—we found that the potency of 3144 correlated with the degree of dependency on the mutated isoform over a 5-fold concentration range, assessed by siRNA-mediated knockdown of the mutated allele (Figure

S3); however, at higher concentrations, other lethal mechanisms may operate. In addition, consistent with the fact that RAS-dependent cells have been reported to die by apoptosis upon RAS knockdown, we found that 3144 induced caspase activity to a similar level as staurosporine, a known apoptosis inducer (Figure S3C). As further confirmation of RAS-dependent lethality, we found that the lethality of 3144 was reduced by overexpression of activated alleles of PI3K and/or BRAF in HT-1080 cells ($NRAS^{Q61K}$), which are downstream effectors of RAS proteins (Figure S3F).

We then evaluated 3144 in primary T-cell acute lymphoblastic leukemia (T-ALL) cells cultured *in vitro*. The compound was tested in two samples containing mutant *NRAS* (G13V and G13D) as well as in four *NRAS* wild-type samples (Figure 3D). Selective lethality was observed, with mutant *NRAS* cells retaining only 20–40% viability after 5 μM treatment, but no observable effect on viability of the four patient samples with wild-type *NRAS* at this concentration. We also tested whether 3144 was able to prevent growth of RAS mutant cancer cells in an anchorage-independent fashion, which is a more physiologically relevant culture condition. The activity of 3144 was assessed by seeding the breast cancer MDA-MB-231 cell line ($KRAS^{G13D}$) and the colorectal cancer SW480 ($KRAS^{G12V}$) in low-adherence plates, resulting in aggregation into tumor-like spheres. Vehicle-treated cells grew into multicellular tumor spheroids that decreased in size in a dose-dependent manner in the presence of the compound (Figure S3D). To examine the relationship between potency in cells compared to in vitro assays, we measured the accumulation of 3144 in DLD-1 cancer cells, and found that the compound accumulates between 60 and 180 fold in cells (Figure S3E), perhaps explaining its greater potency in some cell lines compared to in vitro assays; however, this effect may vary across cell lines.

Inhibition of RAS signaling pathways in cancer cells by 3144

To determine whether the inhibition of RAS-effector interactions and signaling occurs in cell culture, we examined the ability of 3144 to disrupt RAS-PI3K-AKT and RAS-RAF-MEK-ERK signaling. We found that the $Hras^{-/-}; Nras^{-/-}$; $Kras^{flox/flox}$ MEFs showed moderately decreased pERK and pAKT abundance after 3144 treatment for 0.6 h, 1 h or 16 h and that BRAF-CAAX-containing MEFs were more resistant to this effect (Fig. 4A); BJeLR (with $HRAS^{V12}$) engineered tumor cells and HT-1080 fibrosarcoma cells (with $NRAS^{Q61K}$) exhibited somewhat decreased pERK and pAKT abundance upon treatment with 3144 (Figure 4B); 3144 also suppressed to a degree EGF-induced pAKT and pERK abundance in these cell lines (Figure 4B). We found decreased CRAF-bound RAS and RALA-GTP (a marker of the RAL-GDS pathway downstream of RAS proteins, Figure 4C, D) upon 3144 treatment of BJeLR cells. These observation suggested that within a range of concentrations in at least several cell lines, 3144 can partially inhibit RAS signaling and cause a degree of RAS-dependent lethality.

3144 has suitable ADME properties for in vivo testing

We sought to test whether compound 3144 would have an acceptable therapeutic index *in vivo*. Initially, to test whether the compound was sufficiently metabolically stable for *in vivo* testing, 3144 was incubated with purified mouse and human liver microsomes and its degradation was followed by LC-MS; 3144 was relatively stable over 120 minutes in both

human and mouse liver microsomes (Figure 5A). The pharmacokinetics of compound 3144 were measured by analyzing plasma samples from male C57BL6 adult mice after the compound was administered orally (PO), intraperitoneally (IP) or intravenously (IV). After monitoring the concentration of 3144 over 12 hours, we observed suitable pharmacokinetics with all three routes of administration (Figure 5B and Supporting Information), suggesting it would be feasible to test the efficacy of 3144 in mouse cancer models.

3144 prevents the growth of a RAS mutant mouse cancer xenografts

The *in vivo* efficacy of 3144 was initially assessed in a xenograft mouse tumor model using the MDA-MB-231 cell line ($KRAS^{G13D}$) in 8-week-old nude mice starting with relatively small tumors. The compound was administered either orally or via alternating IV and IP injections. Both routes of administration resulted in inhibition of tumor growth over 15 days of treatment (Figure 5C). To evaluate whether 3144 inhibited RAS signaling *in vivo*, we performed a pharmacodynamic study: after six days of treatment, tumors were analyzed for phosphorylated ERK levels (Figure S5E). 3144-treated mice exhibited somewhat decreased tumor pERK tumor levels compared with vehicle-treated mice.

To test the effect of 3144 in a more physiologically relevant patient-derived xenograft cancer model, we used the PDTALL22 patient T-ALL sample as a luciferase-expressing xenograft. Xenografted mice were imaged after 4 and 8 days of 3144 treatment, and a decrease in tumor burden was observed (Figure 5D). Consistent with the decrease in tumor burden, examination of the spleen revealed a decrease in size with inhibitor treatment, as well as a reduction in the percent of infiltrative human CD45+ cells (Figure 5E). Hematoxylin and eosin staining also showed decreased cellularity, consistent with these results (Figure 5F).

3144 causes inhibition of RAS signaling in the $KP^{f/f}C$ mouse model of pancreatic cancer

Mutations in *RAS* genes are found in 90% of pancreatic cancers; pancreatic ductal adenocarcinoma is particularly resistant to chemotherapy, as it is known to have a dense, desmoplastic stroma that can limit drug delivery (Oberstein and Olive, 2013). The most commonly used therapeutic agent, gemcitabine, extends patient survival by only a few weeks (Burris et al., 1997). To test whether 3144 could penetrate these difficult to access tumors, we used the $Kras^{LSL.G12D/+}Tp53^{fl/fl}Pdx1\text{-}Cre$ ($KP^{f/f}C$) mouse model (Bardeesy et al., 2006), which allows for both pancreas-specific expression of $Kras^{G12D}$ and the deletion of p53. This causes the mice to have one functional *Kras* allele in the remaining tissue in which Cre recombinase is not expressed.

Pre-treatment biopsies were acquired from each mouse by abdominal laparotomy, followed by a day of recovery and treatment with 30 mg/kg 3144 via IP injection. Toxicity was observed in the $KP^{f/f}$ C mice, but not in wild-type mice (Figure S5C, D). This resulted in early termination of the study and efficacy was not evaluated. We attribute the toxicity observed in these mice to the presence of only one functional *Kras* allele, making them more sensitive to pan-RAS inhibition. This suggests that due to this genetic manipulation, pan-RAS inhibitors cannot be evaluated for efficacy in mice containing one *Kras* allele.

To test whether compound 3144 inhibited RAS signaling in these mouse pancreatic tumors, we compared pre- and post-treatment tumor samples for markers of RAS inhibition. We

observed a decrease for both pAKT (S473) and pERK1/2 (Figure 5G, H) after 3144 administration. A modest increase in cleaved caspase-3 was also observed, showing that in this model, 3144 has the capacity to induce caspase activation (Figure S5A, B). These data suggest that pan-RAS inhibitors developed using this approach may provide probes and candidate therapeutic agents for pancreatic cancers and other RAS-dependent cancers, although the therapeutic index needs to be evaluated more thoroughly for such an approach.

Discussion

Mutations in the RAS family of genes (*NRAS*, *KRAS* and *HRAS*) are common genetic alterations in many cancers; nonetheless, it has been challenging to directly target these proteins with therapeutic agents. Recently, there has been renewed enthusiasm for the potential feasibility of direct targeting of RAS proteins (Burns et al., 2014; Cox et al., 2014; Maurer et al., 2012; Ostrem et al., 2013; Shima et al., 2013; Spiegel et al., 2014; Stephen et al., 2014; Sun et al., 2012; Sun et al., 2014; van Hattum and Waldmann, 2014; Wang et al., 2012; Ward et al., 2012; Weiwer et al., 2012). We hypothesized that computational and biophysical tools would make it feasible to design and test small molecules that interact with the active, GTP-bound state of RAS proteins, blocking binding of effector proteins. It has been noted that recognizing large areas of a protein surface may require multivalent contacts (Hewitt and Wilson, 2016), and that fragment-based drug discovery provides advantages for challenging target classes (Jahnke and Erlanson, 2006). We found that by designing compounds that are predicted to bind simultaneously to two adjacent sites on RAS proteins, it was possible to generate a ligand that has pan-RAS inhibitory activity. Biophysical assays and mutagenesis suggested that this compound, 3144, binds with an affinity in the micromolar range, albeit with potential additional target binding at higher concentrations. This compound also had suitable physicochemical properties for cell penetration, metabolic stability and *in vivo* administration: we observed that this compound accumulates to a substantial degree in cells in culture, perhaps leading to augmented cellular activity in cells and in mice.

Despite the potential utility of compound 3144 and the approach used in its discovery, we note that we detected toxicity and off-target activity of compound 3144, *in vitro*, in cells and in mice, suggesting that this compound would need to be optimized to create a pan-RAS inhibitor with greater potency and specificity, or that additional scaffolds would need to be explored that achieve the same end. In addition, the water solubility of 3144 is low, making it challenging to use in some contexts. Nonetheless, the results presented here suggest a possibly useful approach to targeting RAS proteins in human cancers that is complementary to the previously reported strategies of designing covalent G12C-mutant-specific or isoform-specific inhibitors. Moreover, we found that despite the importance of *Kras* for normal mouse development, a pan-RAS inhibitor can have a suitable therapeutic index in cell culture and in mouse cancer models, possibly due to the varying degrees of RAS addiction of various normal tissues and cancers, upon which the biodistribution and pharmacokinetic and pharmacodynamic profile of a small molecule inhibitor is superimposed. In the case of compound 3144, this resulted in an anti-tumor effect in mice.

In summary, the results described herein suggest that structure-based design of multivalent small molecule ligands for specific proteins may be feasible. This approach resulted in the discovery of a compound with inhibitory activity in primary patient samples and in murine xenograft models. This may ultimately be a means of disrupting the oncogenic functions of proteins in human tumors.

STAR Methods

CONTACT FOR REAGENT AND RESOURCE SHARING

Further information and requests for resources and reagents should be directed to and will be fulfilled by the Lead Contact Brent R. Stockwell (bstockwell@columbia.edu). Columbia University requires that a material transfer agreement (MTA) be signed for transfer of materials. Plasmids and cell lines will be made available through such MTAs, unless precluded by existing MTAs. Small amounts of non-replicating materials (*e.g.,* compounds) will be made available as reference standards when a sufficient supply is available.

EXPERIMENTAL MODEL AND SUBJECT DETAILS

Animal studies—The animals studies reported in this manuscript adhere to the ARRIVE guidelines. All animal study protocols were approved by the Columbia University Institutional Animal Care And Use Committee (IACUC).

Pharmacokinetic analysis in mice: C57BL/6 male mice of 6–7 weeks of age and ~25 g weight (Charles River, strain 027) were acclimated after shipping for >3 days. Mice were weighed before injection to confirm that all mice were 23–25 g and divided into groups of 3 mice per cage. 30 mg of 3144 was dissolved in 6 mL 10% NMP/90% PEG to create a 5 mg/mL solution. The solution was then sterilized using a 0.2 μm syringe filter. Mice were dosed at 20 mg/kg using three different routes, IP, IV, and PO, and samples were collected at 0.5, 2, 4, 8, 12 h, time points, with three mice per time point. At the appropriate time, mice were sacrificed by CO_2 asphyxiation for 3 min and ~0.5 mL of blood was collected via cardiac puncture. Blood was immediately put into tubes with K2 EDTA anticoagulant and placed on ice. Samples were centrifuged for 10 min at 4 °C and 2,100 × *g*, then plasma was transferred to a clean microfuge tube. Plasma samples were flash frozen in liquid nitrogen and stored at −80°C. Additionally, six mice were used as a control and not treated with compound. Plasma from control mice was used to calibrate LC-MS and correct for matrix affects. 3144 concentration was determined in mouse plasma samples using Ultra High Performance Liquid Chromatography-Tandem Mass Spectrometry (UPLC-MS-MS). 3144 was extracted from plasma by mixing 100 μL of plasma samples with 900 μL of acetonitrile. After mixing for 5 min, the mixture was centrifuged for 10 min, the organic layer was transferred to an UPLC-MS vial, dried under a nitrogen stream and reconstituted in 100 μL of 75% methanol with 5 mm ammonium formate. Calibration standards and quality control samples were prepared spanning a range of 10 ng/ml to 250 ng/ml and extracted in the same manner as the samples. UPLC-MS/MS analysis was performed on a platform comprising a triple quadrupole Waters Xevo TQ-S (Waters, Milford, MA) equipped with an electrospray ionization source and integrated with a Waters Acquity UPLC controlled by Mass Lynx Software 4.1. Chromatographic separation was performed by injecting 5 μL of the extract

onto a Waters C18 BEH column (2.1 × 50 mm, 1.7 μm, 130 Å) maintained at 50 °C. The flow rate was maintained at 500 μL/min. The initial flow conditions were 90% solvent A (water containing 5mm ammonium formate) and 10% solvent B (methanol containing 5 mm ammonium formate). Solvent B was raised to 50% over 3 min and to 98% by 4 min, lowered to 50% by 5 min and back to initial conditions by 6 min with a total run time of 6.5 min. The retention time for 3144 was 4.26 min. The mass spectrometer was operated under multiple reaction monitoring (MRM) mode with positive electrospray ionization with the following parameters: Capillary voltage: 0.8 Kv, cone gas flow: 150 L/h; desolvation gas: 1000 L/h; and gas temperature: 500 °C. For MRM, following transitions were utilized for quantitation: 717.23>456.21 (quantifier ion) and 717.23>330.29 (qualifier ion). Peak integration and data analysis were performed with Target Lynx 4.1. Lower limit of quantification (LLOQ), defined as the lowest concentration with an accuracy and precision of <20% was determined to be 25 ng/ml. The intra-assay precision for the assay was 9.55%. Non-compartmental pharmacokinetics of compound 3144 were assessed using WinNonlin Pharmacokinetics software (Certara, Princeton, NJ). HL_Lambda_z = terminal half-life (h); Tmax = Time to reach the maximum plasma concentration (h); Cmax = maximum plasma concentration reached (ng/mL); Tlast = last observed concentration (h); Clast = last measured concentration (ng/mL); AUClast = Area under the plasma concentration time curve from t = 0 h until the last measured concentration (h*ng/mL); AUCINFobs = Area under the plasma concentration time curve from t = 0 h until infinity, calculated using the calculated half-life and the last measured concentration (h*ng/mL).

	HL_Lambda_z	Tmax	Cmax	Tlast	Clast	AUClast	AUCINF_obs
	h	h	ng/mL	h	ng/mL	h*ng/mL	h*ng/mL
IP	3.6 +− 1.0	0.5 +− 0.9	3500 +− 390	12	81 +− 11	9100 +− 3100	9700 +− 3000
IV	6.9 +− 5.0	0.5 +− 0.0	970 +− 660	12	86 +− 90	2600 +− 1000	3400 +− 3200
PO	>12	4 +− 2	93 +− 37	12	26 +− 9.1	710 +− 2900	5649

Xenograft therapeutic study in mice: Athymic nude Nu/Nu Crl:NU-Foxn1^{nu}, hairless, albino mice (eight weeks old; Charles River Laboratories, Strain 088) were injected with 7 million MDA-MB-231 cells subcutaneously. After 3 d, mice were separated randomly into treatment groups of roughly equal tumor size (58 mm^3) and dosed with 180 mg/kg 3144 orally (12 mg/mL, 10% DMSO, pH 4), vehicle orally, or by a combination of intraperitoneal and intravenous injections at 30 mg/kg (4 mg/mL, 5% DMSO in HBSS at pH 4). Over 14 d, mice received a total of 10 doses of 3144 or vehicle orally, or six intraperitoneal injections and 4 intravenous injections. Tumor size was measured by electronic caliper every 2 d and calculated using the formula: 0.523 × length × width^2.

Pharmacodynamic study using MDA-MB-231 cells: Athymic nude mice (eight weeks old; Charles River Laboratories) were injected with 8 million MDA-MB-231 cells subcutaneously. After 4 d, mice were separated into treatment groups of roughly equal tumor size (128 mm^3) and population, and dosed with 30 mg/kg 3144 in 5% DMSO HBSS at pH 4 or vehicle (5% DMSO HBSS at pH 4) intraperitoneal, once per day for 6 d. Tumor size was

measured by electronic caliper every 2 d and calculated using the formula: 0.523 × length × width^2. Mice were euthanized using a CO_2 gas chamber before xenograft dissection. Tumors were then weighed, frozen and stored at −80°C. Segments of the tumor (~60 mg) were suspended in 120 uL lysis buffer. Xengrafts were then lysed by sonication (40 amp for 10–15 seconds) and samples were centrifuged at 14,000 rpm at 4°C for 30 min to remove unlysed cells and debris. The supernatant was then analyzed by western blotting.

Patient-derived xenograft study: For this study, animals were maintained in the animal facility at the Irving Cancer Center at Columbia University Medical Campus. Species: *Mus musculus* (mouse); Strain: Rag2- γc-; Sex: Female; Age: 4 weeks; Weight: 22–24g; Genotype:Il2rg$^{tm1.1Flv}$ Rag2$^{tm1.1Flv}$; Vendor: Jackson Laboratories; Catalog number: 014593 | Rag2- γc-; Housing: 5 animals per cage. To generate primary xenografts, cells from T-ALL sample PD22, harboring a mutated allele of *NRAS*, were transplanted via intravenous injection into lethally irradiated primary recipient mice (Chiang et al., 2008). Upon detection of human lymphoblasts (human CD45+ cells) in peripheral blood, mice were sacrificed; lymphoblasts isolated from the spleens were transduced with retroviral particles expressing a fusion protein between the red cherry fluorescent protein and luciferase (MigR1 CherryLUC), and re-injected in sublethally irradiated mice (Piovan et al., 2013). Mice transplanted with retrovirally transduced cells were imaged regularly until luciferase activity was detected. Tumor cells were harvested from the spleens of these mice, and injected into secondary recipient mice. Secondary recipients were randomized into two groups of 5 mice with equal load of luciferase. Animals were treated intraperitoneally with vehicle or 3144 at 30 mg/kg in 5% DMSO in HBSS at pH 4., once daily on days 0, 1, 4, 5, 7 and 8, and imaged at day 0 (before treatment), at day 4 and at day 8. Mice were sacrificed at day 8; spleen weight and presence of human CD45+ cells in the spleen (lymphoblasts) were documented together with changes in luciferase signal over treatment.

KP$^{f/f}$C mouse pharmacodynamic study: KRAS$^{LSL\ G12D}$; p53$^{fl/fl}$; Pdx1-Cre (KP$^{f/f}$C) mice have been previously described (Bardeesy et al., 2006). Animals were housed in a barrier facility and monitored daily prior to enrollment on studies. KP$^{f/f}$C were palpated twice weekly to assess for tumor formation. Upon discovery of a palpable mass deemed amenable to surgery, tumors were accessed by abdominal laparotomy as previously described for biopsy procedures (Sastra and Olive, 2014). In short, mice were anesthetized with isofluorane, prepared for aseptic surgery, and injected with buprenorphine intra-operatively to initiate post-operative analgesia. Following visual identification, tumors were held in place with a pair of biopsy forceps while a small-diameter biopsy punch (2-mm diameter, Zivic Instruments PUN2000) was used to cleanly remove a tissue sample. The resultant wound was filled with an absorbable, gelatin-compressed sponge to staunch possible bleeding. Incisions were sutured closed and the mouse was allowed to recover from 24–48 h prior to study initiation. Biopsy samples derived from small animal surgery were divided in two specimens. The first was stored in 10% buffered formalin phosphate overnight at 4 °C and then placed in 70% ethanol for extended storage prior to processing and embedding in paraffin wax blocks. The second was embedded in O.C.T. compound and subsequently frozen atop a bath of liquid N_2 prior to long-term storage at −80°C. Tumor samples taken at necropsy were processed and stored identically to those described above. Paraffin embedded

samples were sectioned at 5 μM thickness and mounted on positively charged sample slides. These slides were heated at 60 °C for 15–30 minutes and subsequently rehydrated by standard protocols. Unmasking was performed in 10 mM citrate buffer, pH 6.0 for 5 minutes in a pressure cooker at high temperature, followed by peroxidase quench in 3% hydrogen peroxide for 20 minutes. Blocking was carried out using 1.5% horse serum and 2% animal free blocker (Vector Labs) in TBS-T for 1 hour at room temperature. Slides were incubated with primary antibody (cleaved caspase-3, catalog no. 9664; ERK, catalog no. 4695; pERK, catalog no. 4376; all antibodies from Cell Signaling) overnight at 4 °C. Slides were then allowed to equilibrate to room temperature prior to washing with TBS-T and incubation with secondary antibody (ImmPress polymer reagent, Vector Labs). Signal was developed with ImmPACT DAB Peroxidase Substrate (Vector Labs). Slides were counterstained with hematoxylin for 30 seconds. For quantification of cleaved-caspase 3 staining, all available 40× fields on three separate sections of biopsy samples and 20 different 40× fields from two separate sections of necropsy samples were analyzed for each study mouse. Mice were dosed once daily with 40 mg/kg of 3144 in 5% DMSO in Hanks' Balanced Salt Solution at pH 4.0, via IP injection. Mice were monitored for changes in health and were sacrificed after 5 d on study or once they met endpoint criteria in keeping with IACUC standards.

WT mouse weights

days on study	M205	M206	M207	M208	M287
1	21.36	20.39	22.08	23.6	25
2	20	18.8	20.6	22.7	23.38
3	20	18.4	20.1	21.87	22.16
4	20.77	17.4	19	21.08	23
5	20.78	17.27	18.6	21.4	22.18

K mouse weights

days on study	K8225	K8279	K8266	K8267	K8282
1	19.1	14.5	22.9	26.1	18.5
2	18.4	14.1	21.6	24.7	17.4
3	18.6	14.2	20.7	23.6	17
4	17.5	14.2	20.1	23.27	17.7
5	17.5	13.63	19.8	22.7-x	16.5

KC mouse weights

days on study	K8072	K8069	K8073	K7923	K7916
1	33	30.5	30.7	33.5	35.8
2	32.2	28.1-x	27.8	33.5	34.5
3	29.9		24.84	32	26.86-x
4	28.8		23.6-x	30.5	
5	28.5			30.2	

x indicated day on which animal was sacrificed due to reaching endpoint criteria

Human patient T-ALL samples—T-ALL samples were provided by Columbia Presbyterian Hospital, the Eastern Cooperative Oncology Group (ECOG), University of Padova, and Hospital Central de Asturias with informed consent and analyzed under the supervision of the Columbia University Medical Center Institutional Review Board committee. For the analysis of 3144 on primary T-ALL patient samples, cells were cultured medium supplemented with 10% FBS, 10% human heat-inactivated serum, 1% penicillin/streptomycin, 1% GlutaMAX, human IL-7 (10 ng/mL), human SCF (50 ng/mL), human FLT3-ligand (20 ng/mL), and insulin (20 nmol/L) on a feeder layer of MS5 stromal cells overexpressing the NOTCH ligand Delta-like 1. In these experiments, 250,000 T-ALL lymphoblasts were cultured in each well of a 24-well plate in triplicate and treated with either vehicle (DMSO), or 3144 (ranging from 1 to 5 μM). We harvested the cells 72 h after treatment and analyzed cell viability using the BD cell viability kit with liquid counting beads (BD Bioscience), gating out stromal cells (GFP+), dead cells and particles (defined as PI+). We acquired data using a FACSCanto II flow cytometer (BD Bioscience) and analyzed it using FlowJo software (Tree Star, Inc.). Viability data are represented as percent relative to vehicle treatment. A region of 124 bp from coding exon 1 of the human *NRAS* gene, including G12–G13 mutation hotspot, was amplified from the genomic DNA of six primary T-ALL samples by polymerase chain reaction and was analyzed by direct dideoxynucleotide sequencing using primers FW: 5′-GCTGGTGTGAAATGACT-3′ and. RV: 5′-GCTACCACTGGGCCTCACCT-3′. PDTALL 22 synonymous variants GCA/GCT (A); GGT/GTT (G13) (G13V). PDTALL26 missense variant GGT/GAT (G13) (G13D).

Cell lines and bacterial strains

Sources of cell lines: Phoenix-AMPHO cells were from ATCC (catalog number CRL-3213). *Kras*$^{lox/lox}$, *Hras*$^{-/-}$, *Nras*$^{-/-}$ *RERTn*$^{ert/ert}$ mouse embryo fibroblasts (MEFs) were from the laboratory of Mariano Barbacid (#DU315–6) and were authenticated by blotting for RAS proteins. *Hras*$^{-/-}$; *Nras*$^{-/-}$; *Kras*$^{lox/lox}$ BRAF(V600E)-CAAX MEFs were generated as described below. DLD-1 colon cancer cells were from ATCC (catalog number CCL-221). MDA-MB-231 cells were from ATCC (catalog number HTB-26). BL21-Gold (DE3) competent *E. coli* cells were from Stratagene (catalog number 230132). Cell lines obtained from ATCC were not further authenticated.

Generation of RAS-less Mouse Embryo Fibroblasts expressing BRAF^{V600E}-CAAX: A BRAF^{CAAX} plasmid was created by inserting a CAAX motif (cloned from pLL7.0: Venus-iLID-CAAX, Addgene, Plasmid #60411) into pBabe-Puro-BRAF-V600E plasmid (Addgene, Plasmid #15269). pBABE-puro plasmid was obtained from Addgene, Plasmid #1764. Retroviruses were generated by transfection of plasmids into Phoenix-AMPHO (ATCC: CRL-3213) cells using Lipofectamine 2000. The retroviruses were transfected into *Hras*$^{-/-}$; *Nras*$^{-/-}$; *Kras*$^{lox/lox}$ MEFs (from Mariano Barbacid) followed by 2 weeks of puromycin (1 ug/mL) selection. MEFs transfected with empty pBABE-puro were used in Presto blue assays and western blotting. To generate BRAF^{CAAX} MEFs, the MEFs were then cultured in the presence of (*Z*)-4-hydroxytamoxifen (4OHT) (Sigma, 600 nM) for another 2 weeks to remove the endogenous *Kras*. The obtained BRAF^{CAAX} MEFs were then used in Presto blue assays and western blotting. Phoenix-AMPHO (ATCC: CRL-3213) cells were seeded in a 6-well plate at 800,000 cells/well in 10% fetal bovine serum (FBS), 1% PS,

and 2 mM L-glutamine in DMEM. After 20 h, the medium was changed to 800 uL Opti-mem in each well. A solution of Lipofectamine 2000 (6 μL) in 100 μL Opti-mem media (reduced serum media) and the plasmid (2.5 μg) in 100 μL Opti-mem media were combined and incubated 20 min at 25 °C, then added to each well. After 4 h, 1 mL Opti-mem with 20% FBS was added to each well. 24 h later, the medium was replaced with 10% FBS, 1% P/S, 2 mM L-glutamine in DMEM. The next day the supernatant was collected three times spaced 4 h apart and polybrene was added (1/1000). The supernatant was filtered (0.45 μm filters) and added to MEFs seeded at 160,000 cells per well (6-well dish) in 2 mL portions spaced 4 h apart. After 48 h, the cells were trypsinized and re-seeded in medium containing puromycin (1 μg/mL). After 2 weeks of selection with puromycin, the MEFs were cultured in the presence of (*Z*)-4-hydroxytaoxifen (4OHT) (Sigma, 600nM) for another 2 weeks to ablate the endogenous *Kras*. The MEFs were then used in Presto-blue assay and western blot. CAAX motif sequence:
CATAATTACACACTTTGTCTTTGACTTCTTTTTCTTCTTTTTGCTCCCACTCCCGCTTCC

METHOD DETAILS

Viability assay in Mouse Embryo Fibroblasts—Mouse embryo fibroblasts in which *Nras* and *Hras* had been deleted and only one floxed allele of *Kras* remained (DU315–6, gift from Mariano Barbacid) were transfected with either empty vector or a $BRAF^{V600E}$ expression vector and 4-OHT selection to eliminate *Kras*, as described above. Cells were trypsinized, counted, and seeded into 384-well plates at 30,000 cells/well in serum-free medium. After 16 h, compounds (from 10 mM stocks in DMSO) were arrayed in a 10-point 2-fold dilution series in 384-well polypropylene plates. Compound solutions were transferred at a 1:5 dilution into assay plates. After 48 h, a 50% Presto blue solution was added to a final concentration of 10% Presto blue. After 6 h of incubation, fluorescence intensity was determined using a Victor3 plate reader (Perkin Elmer) with a 535 nm excitation filter and a 590 nm emission filter. All compound measurements were performed in duplicate.

Western blots of Mouse Embryo Fibroblasts—0.25 million cells/well were seeded in DMEM with 1× Glutamax, 10% heat-inactivated FBS, and 1% P/S. After the cells grew to 80% confluence, the medium was changed to serum-free medium, and the cells incubated for 24 h. The medium was changed to serum-free medium with compounds (5 μM 3144 for 35 min, 1 h or 2 μM 3144 for 16 h to prevent the cells from dying before protein could be extracted at 16h). The cells were stimulated with human EGF (10 ng/ml) for 15 min to stimulate RAS-dependent pERK and pAKT signaling. Then the cells were washed with cold PBS and lysed. For quantitation, the background value of the scanned gel was subtracted, and the relative abundance was determined by:

pErk = (pErk/Tubulin)/(total Erk/Tubulin)

pAkt = (pAkt/Tubullin)/(totalAkt/Tubulin)

which was then normalized to the DMSO control.

Pan-RAS siRNA knockdown and treatment with 3144—DLD-1 cells were reverse transfected with siRNA pools targeting three RAS isoforms (*HRAS*, *KRAS*, *NRAS*) following manufacturer's instructions. In brief: for each well of a 6 well plate, 3.33 μL each of SMARTpool: ON-TARGETplus siRNAs (10mM; Dharmacon) targeting *HRAS*, *KRAS*, and *NRAS* were combined into 250 μL of Opti-mem serum-free media in a 1.5 mL Eppendorf microfuge tube. In a separate tube, 6 μL of Lipofectamine RNAi/MAX was added to 250 μL of Opti-mem media, and both tubes were allowed to equilibrate at RT for 5 min. The contents of the two tubes were combined, and dispensed into wells of a 6-well plate and incubated for 20 min at 37 °C. To evaluate whether siRNAs affect cell viability or the response to 3144, a control group of DLD-1 cells was transfected with an equivalent volume of ON-TARGETplus Non-targeting Pool siRNAs (Dharmacon), following the same method. After incubation, 2 mL of DLD-1 cells growing in RPMI media (10% FBS, 1% P/S) were added to each well at a concentration of 0.125×10^6 cells/mL. The plate was incubated for 72 h, after which the cells were washed with PBS, trypsinized, resuspended in RPMI media (10% FBS, 1% P/S), and counted on a Vi-Cell XR Cell Viability Analyzer (Beckman Coulter). At this time, approximately 1×10^6 cells were sampled to evaluate RAS knockdown via western blot. Remaining cells were spun down at 125 × g for 5 min, after which the pellet was re-suspended in serum-free RPMI medium at 0.277×10^6 cells/mL. From this, 36 μL was added to each well in a 384-well plate, totaling 10,000 cells/well, and plates were incubated overnight. The following day, dilution series of 3144 and MG132 were created in Opti-mem serum-free media at a 10× concentrated stock solution. 4 μL was then added to each well of the 384-well plate, totaling 40 μL final volume in each well. The 384-well plate was incubated for 24 h, after which cell viability was measured using the CellTiter-Glo® Luminescent Cell Viability Assay (Promega).

Microsomal Stability Assay—To an Eppendorf microfuge tube was added phosphate buffer (182.2 μL, pH 7.4, 100 mM) followed by addition of NADPH-regenerating system system solution A (10 μL), and NADPH regenerating system solution B (2 μL) (Corning Gentest 3P NADPH regenerating system solution A (#451220) and B (#451200)). A stock solution of 3144 (0.8 μL. 5 mM) or 7-ethoxycoumarin (positive control, 0.8 μL, 5 mM) was added and the mixture was warmed to 37 °C for 5 minutes. Mouse microsomes (CD-1, 20 mg/mL, Life Technologies) or human microsomes (pooled 50 donors, 20 mg/mL, Thermo Fisher Scientific) (5 μL, thawed in 37 °C water bath before use) were added. At selected time points (0, 15, 30, 45, 60 and 120 minutes) aliquots (15 μL) were withdrawn from the tube and quenched upon addition to cold acetonitrile (60 μL), containing an internal standard (5 μM) in an Eppendorf microfuge tube. The samples were centrifuged at 13,000 rpm for 10 minutes at 4 °C. The supernatant (40 μL) was withdrawn and transferred to a sample vial with insert. The samples were analyzed by LC-MS. LC-MS analysis was performed on a platform comprising a Thermo Scientific Dionex Ultimate 3000 and a Bruker amaZon SL equipped with an electrospray ionization source controlled by Bruker Hystar 3.2. Chromatographic separation was performed by injecting 5 μL of the sample onto an Agilent Eclipse Plus C18 column (2.1 × 50 mm, 3.5 μm) maintained at 20 °C. The flow rate was maintained at 400 μL/min. The initial flow conditions were 60% solvent A (water containing 0.1% acetic acid) and 40% solvent B (methanol containing 0.1% acetic acid). Solvent B was raised to 60% over 0.25 minutes and to 70% by 6.75 minutes. Solvent B was raised to 95%

by 7.00 minutes and lowered back to initial conditions (40%) by 8.00 minutes with a total run time of 9.00 minutes. The retention time for 3144 was 1.7 minutes.

Software and Computational Methods—Molecular docking and modeling was performed using Glide (versions 2012–2016, Schrödinger, Inc.) and Molecular Operating Environment [MOE] (Chemical Computing Group). All chemical structures were drawn using ChemDraw Ultra version 10.0 (Perkin Elmer). All statistical analyses, potency determinations, and viability curves were produced using Prism 5.0c (GraphPad Software). Libraries of commercially available compounds were compiled from the inventories of Asinex, Enamine, Chembridge, ChemDiv, IBS, Life, Maybridge and TimTec. A fragment subset of ~60,000 compounds was selected using the following filter criteria: LogP <3, hydrogen bond acceptors ≤ 3, hydrogen bond donors ≤ 3, molecular weight <300, aqueous solubility > 0.5 mM. Chemical descriptors were calculated using MOE (Chemical Computing Group). Designed libraries of synthetically accessible compounds were compiled using selected commercially available reagents from the inventory of Sigma-Aldrich and Chem-Impex using the Combigen application in MOE (Chemical Computing Group).

Solubility of compound 3144—We saw no visible precipitation of compound 3144 up to 250 μM in aqueous buffers (*e.g.*, phosphate buffered saline) at room temperature with 1.5% DMSO. However, solubility in aqueous solutions was often less than anticipated based on measured concentrations in solution, sometimes as low as 5 μM.

Cell viability assays—Cell culture assays were incubated at 37°C with 5% CO_2, using media recipes specified by ATCC. For 384-well cancer cell viability assays, cells were trypsinized, counted, and seeded into 384-well plates at 1,000 cells/well, unless otherwise specified. After 16 h, compounds (from 10 mM stocks in DMSO) were arrayed in an 8-point or 16-point dilution series in 384-well polypropylene plates. Compound solutions were transferred at a 1:5 dilution into the assay plates. After 48 h, a 50% Alamar blue solution was added to a final concentration of 10% Alamar blue. After 6 h of incubation, fluorescence intensity was determined using a Victor3 plate reader (Perkin Elmer) with a 535 nm excitation filter and a 590 nm emission filter. All 384w measurements were performed in triplicate. For 6 well format, cells were trypsinized, counted, and seeded into 6-well plates at 200,000 cells per well 16 h prior to use. Medium was then aspirated and replaced with 2 mL of media containing compounds at the indicated concentrations (from 10 mM stocks in DMSO). After 24 h, cells were trypsinized and viability was determined using Trypan Blue exclusion (Vi-Cell).

Western blots—Cells were seeded in DMEM and 10% FBS with 1% penicillin and streptomycin (PS) or DMEM and 2% FBS with 1% penicillin and streptomycin (P/S), 16 h prior to use. The medium was then aspirated and compounds added as solutions in serum free medium (DMEM with 1% PS) or DMEM and 2% FBS with 1% penicillin and streptomycin (PS) to the dishes and treated at the indicated time points. Following treatment, the medium was aspirated from each dish and cells washed twice with PBS. Cells were lysed with 60 μl buffer (50 mM HEPES, 40 mM NaCl, 2 mM EDTA, 0.5% Triton-X, 1.5 mM

sodium orthovanadate, 50 mM NaF, 10 mM sodium pyrophosphate, 10 mM sodium β-glycerophosphate and protease inhibitor tablet (Roche), pH 7.4). Unlysed cells and debris were pelleted for 12 min at 12,000 rpm at 4° C. Samples were separated using SDS-PAGE and transferred to a polyvinylidene difluoride membrane. Transfer was performed using the iBlot system (Invitrogen). Membranes were treated with Li-COR Odyssey blocking buffer for 1 h at 25°C, then incubated with primary antibody (1:1000) in a 1:1 solution of PBS-T and Li-COR odyssey blocking buffer overnight at 4°C. Following three 5 min washes in PBS-T, the membrane was incubated with secondary antibodies (1:2000) in a 1:1 solution of PBS-T and Li-COR Odyssey blocking buffer for 45 min at 25 °C. Following three 5 min washes in PBS-T, the membrane was scanned using the Li-COR Odyssey Imaging System. Antibodies for pERK1/2, ERK1/2, pAKT ser473, AKT, pan-RAS, Technology, PI3Kgamma (Cell Signaling), and RAF-1 (Santa Cruz) were detected using a goat anti-rabbit or goat anti-mouse IgG antibody conjugated to an IRdye at 800CW and 680CW conjugated, respectively (Li-COR Biosciences).

Molecular cloning, protein expression, and purification—Human *KRAS4B* sequence containing the oncogenic Q61H mutation in pENTR221 vector was purchased from Invitrogen (Ultimate ORF Clone IOH9852). To generate the wild-type *KRAS* sequence, H61Q back mutation was introduced using QuikChange II site-directed mutagenesis (Agilent Technologies) and confirmed by DNA sequencing (GeneWiz, Inc.). Wild-type *KRAS4B* sequence encoding the catalytic domain (amino acids 1–169 in KRAS) was amplified by PCR and cloned into *Nde I-BamH I* sites of pET-15b vector (Novagen) containing the N-terminal His_6 tag. A G12D point mutation was introduced using QuikChange II site-directed mutagenesis (Agilent Technologies). DNA sequencing was performed to confirm the correct amino acid sequence of the construct (GeneWiz, Inc.). Mutagenesis of the $KRAS^{G12D}$ plasmid was performed using a QuikChange XL site-directed mutagenesis kit. Primers were designed using the Agilent QuikChange Primer Design application and purchased from Integrated DNA Technologies. $KRAS^{G12D\ D38A}$ forward primer 5′ ATA TGA TCC AAC AAT AGA GGC TTC CTA CAG GAA GCA AGT AG 3′, $KRAS^{G12D\ D38A}$ reverse primer 5′ CTA CTT GCT TCC TGT AGG AAG CCT CTA TTG TTG GAT CAT AT 3′, $KRAS^{G12D\ I36N}$ forward primer 5′ CAT TTT GTG GAC GAA TAT GAT CCA ACA AAT GAG GAT TCC TAC AGG 3′, $KRAS^{G12D\ I36N}$ reverse primer 5′ CCT GTA GGA ATC CTC ATT TGT TGG ATC ATA TTC GTC CAC AAA ATG 3′. DNA sequencing was performed to confirm the correct amino acid sequence of the construct (GeneWiz, Inc.).

Nucleotide exchange—Nucleotides in endogenous recombinant KRAS were exchanged with GDP, GTP or GppNHp using an EDTA-loading procedure. $KRAS^{G12D}$ protein (250 μM final) was incubated with 40-fold molar excess of EDTA (10 mM final), and 75-fold molar excess of new nucleotide (18.75 mM final) for 2 h at 30 °C. After incubation, the sample was put on ice for two min and then $MgCl_2$ was added (65 mM final) to stop the reaction. To remove excess unbound nucleotide, the sample was added to a NAP-5 column (GE Life Sciences) equilibrated with Buffer A (25 mM HEPES, 100 mM NaCl, 2 mM TCEP, pH 7.5) and eluted with Buffer A at three drops per fraction. Eluted fractions were evaluated using a Bradford dye-binding method for the presence of protein and those

containing protein were concentrated. For NMR studies, the samples were buffer exchanged into NMR Buffer (50 mM HEPES, 50 mM NaCl, 2 mM TCEP, 2 mM MgCl2, pH 7.4) using a Millipore spin column (13,900 × *g* for seven min at 4 °C, repeated six times, each time adding fresh buffer and discarding the flow-through). Protein concentration was determined using absorbance at 280 nm with extinction coefficient of 11920 M^{-1} cm^{-1} (calculated using ExPASy ProtParam tool).

Cell-based RAS pulldown—BJeLR cells were seeded 16 h prior to use in 10% FBS in DMEM. The medium was then aspirated and replaced with serum-free medium containing the inhibitors (from 10 mM DMSO stocks) and cells were incubated for 24 h. The medium was removed, washed with cold PBS, lysed and spun down at 13,000 rpm at 4 °C to remove unlysed cells and debris. The lysate was incubated with Raf-1 RBD agarose beads (EMD Millipore) for 2 h with rotation at 4°C. The solution was then spun down at 1500 × *g* and the supernatant removed. The beads were washed 2× with PBS, resuspended in 2.5 × SDS, and then analyzed by western blotting procedure.

Determining cellular concentrations of compound 3144—DLD-1 cells were grown in RPMI media containing 10% FBS and seeded in 6-well plates at a density of 0.4×10^6 cells/well, followed by overnight incubation. On the following day, the growth medium was removed and the cells were rinsed twice with PBS, then RPMI growth medium was added, either with or without 10% FBS. Cells were treated for 4 h with 3144 (0.5 μM or 5 μM). After treatment, the growth medium was removed and cells rinsed with PBS, trypsinized and suspended in serum-free RPMI medium. Cells were counted on a Vi-Cell XR Cell Viability Analyzer (Beckman Coulter), and the average diameter was recorded. An aliquot of the appropriate volume of cell suspension (1.0×10^6 cells per sample) was transferred to a 15 mL Falcon tube (3 samples each). The cells were pelleted at 1,000 × *g* for 5 min. The cells were washed twice with PBS and transferred to a 1.5 mL Eppendorf microfuge tube. The cells were pelleted at 3,000 rpm for 3 min, after which the PBS was removed and the pellet frozen at −80°C.

The cell pellet was defrosted and 150 μL of methanol/acetonitrile (1:1) was added, the suspension sonicated for 10 sec, and the compound extracted overnight at 4°C. The samples were spun at 1,400 × *g* for 75 min at 4°C, and the supernatant (75 μL) was withdrawn and transferred to a sample vial with insert. The samples were analyzed by liquid chromatography mass spectrometry (LC-MS). LC-MS analysis was performed on a platform comprising a Thermo Scientific Dionex Ultimate 3000 and a Bruker amaZon SL equipped with an electrospray ionization source controlled by Bruker Hystar 3.2. Chromatographic separation was performed by injecting the sample on an Agilent Eclipse Plus C18 column (2.1 × 50 mm, 3.5 μm) at 20 °C. The flow rate was maintained at 400 μL/min. The initial flow conditions were 60% solvent A (water containing 0.1% acetic acid) and 40% solvent B (methanol containing 0.1% acetic acid). Solvent B was raised to 60% over 0.25 minutes and to 70% by 6.75 minutes. Solvent B was raised to 95% by 7.00 minutes and lowered back to initial conditions (40%) by 8.00 minutes with a total run time of 9.00 minutes. The retention time for 3144 was 1.7 minutes. The peak area was converted to a concentration using a

standard curve and the intracellular concentration was determined using the formula (Colletti et al., 2008):

$$Cellular\ Concentration = Sample\ Concentration \times \frac{Sample\ Volume}{(number\ of\ Cells)(Cell\ Volume)}$$

Microscale thermophoresis (MST) with KRAS^{G12D}—KRAS^{G12D} (250 μM) in 25 mM HEPES, 100 mM sodium chloride, 20 mM EDTA and 1 mM GppNHp was shaken at 220 rpm at 30 °C to remove the endogenous nucleotide. The solution was placed on ice for 2 min prior to the addition of 65 mM $MgCl_2$. After an additional 10 min incubation on ice, 200 μL of a 10 μM solution of KRAS^{G12D} was combined with 200 μL of a 20 μM solution of NT-647-NHS-ester dye (from a 652.4 μM stock). The protein/dye mixture was rotated at 4°C for 30 min, before being separated from the excess dye and buffer exchanged into 25 mM Tris, 100 mM sodium chloride, 2 mM TCEP, and 5 mM $MgCl_2$ via a NAP-5 column. The compounds were arrayed across a 16-point dilution series consisting of 1.5% DMSO with 25 mM Tris, 100 mM NaCl, 2 mM TCEP, 5 mM $MgCl_2$ and 0.05% Tween-20. Thermophoretic movement of the fluorescently labeled protein with the inhibitors was performed using a Monolith NT.115 (Nanotemper Technologies). It is formally possible that ligands such as 3144 induce the formation of an inactive GDP conformation of RAS proteins, resulting in the loss of effector binding.

MST experiments with RAS GTPases—RALA and RHOA were obtained from Abcam (RALA CN:ab102555, RHOA CN:ab101594). RRAS, RRAS2, and RAP1A were purchased from ProSpecBio. KRAS^{WT} and NRAS^{WT} were purchased from Cell Biolabs. HRAS^{WT} was acquired from Enzo Life Sciences. To load GppNHp nucleotide, each GTPase (10 μM final) was incubated with 100-fold molar excess of EDTA (1 mM final), and 1000-fold molar excess of GppNHp (10 mM final) for 2 h at 30 °C. After incubation, the sample was put on ice for 2 min and then $MgCl_2$ was added (65 mM final concentration) to stop the reaction. Excess nucleotide and TCEP was removed using 10 kDa Millipore spin column (13,900 × *g* for 7 min at 4°C, repeated six times) and buffer exchanged into Buffer C (25 mM HEPES pH 7.5, 100 mM NaCl). Protein concentration was determined using absorbance at 280 nm and extinction coefficient determined for each protein based on its sequence. For fluorescence labeling of proteins, a cysteine-reactive dye, NT-647-Red-Maleimide (Nanotemper Technologies), was dissolved in PBS+T buffer (PBS with 0.05% Tween-20) to make a 705 μM stock and added at five molar excess to protein solution. The protein/dye mixture was rotated at 4 °C for 24 h. To remove excess unbound dye, the sample was added to a NAP-5 column (GE Life Sciences) equilibrated with PBS+D buffer (PBS with 3 mM DTT) and eluted with PBS+D buffer at three drops per fraction. The first four eluted fractions were combined and further washed with PBS+D buffer using Millipore spin column (13,900 × *g* for 7 min at 4°C, repeated three times). The binding affinity between 3144 and GTPases-labeled with NT647 was analyzed on a Monolith NT.115 instrument (Nanotemper Technologies). 16-point serial dilutions of compound 3144 were prepared in MST buffer (PBS with 3 mM DTT, 0.05% Tween-20, and 0.2% Prionex) supplemented with 1.5% DMSO and mixed 1:1 with GTPase solution in final volume of 20 μL. Reaction mixture were loaded into standard treated capillaries and analyzed by MST at 40% MST

power and 95% LED power with a laser-on time of 5 sec. The K_D was calculated by taking the average of triplicate F_{norm} measurements at each concentration and fitting the data to a sigmoidal four parameter fitting function in Prism (GraphPad Software).

Differential Scanning Fluorimetry—A fluorescent thermal shift assay was used to confirm the success of nucleotide exchange procedure of all GTPases used in the study. The assay was carried out in triplicate in Fast 96-well optical plates containing 5 μM protein and 5× SYPRO Orange dye (Invitrogen) in 20 μL total volume/well. Samples were heated at 3°C/min from 25°C to 95°C and protein unfolding was observed by monitoring the fluorescence of SYPRO Orange dye at 470 nm excitation and 623 nm emission using ViiA7 real-time PCR machine (Applied Biosystems). Each GTPase with endogenous nucleotide was used on the same plate as a reference for the shift in melting temperature (T_m) with the new nucleotide. All experiments were performed in triplicate. Data were analyzed using Protein Thermal Shift™ Software (Applied Biosystems) to determine the T_m of each well.

^{19}F NMR Spectroscopy—^{19}F NMR experiments were performed on Bruker Avance III 400 (400 MHz) spectrometer (Columbia University) at 300°K in FPLC buffer (25 mM Tris-HCl pH 8, 100 mM NaCl, 5 mM $MgCl_2$, and 1 mM TCEP) with 10% D_2O. Potassium fluoride (KF) and trifluoroacetic acid (TFA) were used as internal standards in all samples.

Isothermal titration calorimetry (ITC)—All ITC experiments were carried out at 25°C on MicroCal Auto-ITC_{200} system (GE Healthcare). Due to low solubility of 3144 in aqueous buffers, the compound was loaded into a cell and the $KRAS^{G12D}$•GppNHp protein was loaded into a syringe. Working stocks of compound 3144 were prepared in 100% DMSO at 20 mM. 450 μL of the compound solution was loaded into cell at 200 μM in ITC buffer (25 mM Tris pH 8.0, 1 mM TCEP, 100 mM NaCl, 5 mM $MgCl_2$, 0.05% Tween-20) with final DMSO concentration at 1.25% (v/v). $KRAS^{G12D}$•GppNHp was buffer exchanged into same ITC buffer using Amicon Ultra 10 kDa size exclusion filter spin columns (buffer replaced with ITC buffer four times). Prior to loading 130 μL of $KRAS^{G12D}$•GppNHp into the syringe at 2.0 mM, DMSO was added to match the amount of DMSO present in the cell. ITC titration experiments were carried out at 25°C with 19 injections, 2 μl per injection, and 180 seconds between each injection. Reference cell power was set to 5 μcal/sec. Control experiments were performed in which ITC buffer was titrated into compound 3144 alone to account for heat released due to dilution. This background was subtracted from test data before final dissociation constant was calculated. Data were analyzed using a one-site binding model in Origin 7.1 software. The dissociation constant, K_D, was calculated according to equation $\mathbf{K_D = 1/K_A}$. Gibbs free energy, **ΔG**, was calculated from equation $\mathbf{\Delta G = -RTlnK_A}$. In addition, **−TΔS** was calculated from equation **ΔG = ΔH−TΔS**. All other parameters, $\mathbf{K_A}$, **n**, **ΔH**, were determined from the titration data.

Protein NMR Spectroscopy—Uniformly ^{15}N-labeled $KRAS^{G12D}$ protein with N-terminal His_6 tag was prepared. The *$KRAS^{G12D}$* construct was expressed in *Escherichia coli* BL21-Gold (DE3) cells (Stratagene) growing at 37 °C in M9 minimal medium supplemented with 100 μg/mL ampicillin, 2 mM $MgSO_4$, 100 μM $CaCl_2$, 1× trace metals, 1× RPMI 1640 vitamin stock (Sigma-Aldrich, cat. R7256), 10 μg/mL biotin, 10 μg/mL

thiamine hydrochloride, and 3 g/L $^{15}NH_4Cl$ as the sole nitrogen source. When OD_{600nm} reached 0.9, protein expression was induced with 1 mM isopropyl β-D-thiogalactoside at 15 °C overnight. Cells were pelleted and lysed by sonication in buffer containing 10 mM Tris-HCl, 500 mM NaCl, 5 mM imidazole, 5 mM $MgCl_2$, pH 7.5, 0.5 % CHAPS (w/v), protease inhibitor tablet (Sigma-Aldrich, cat. 11836170001), and 1 mM TCEP. Cell lysate was then centrifuged at 15,000 × g for 45 min at 4 °C. $KRAS^{G12D}$ was first purified from cell lysate using Ni Sepharose 6 Fast Flow beads (GE Life Sciences) and then using a gel filtration Superdex 100 column. The fractions containing $KRAS^{G12D}$ were pooled together and verified by SDS-PAGE. Thrombin was added at 5 U/mg protein to cleave the N-terminal His_6 tag. The reaction was allowed to proceed overnight at 4 °C. The next day, protein solution was passed over Ni-Sepharose 6 Fast Flow beads (GE Life Sciences) and flowthrough containing the ^{15}N-labeled $KRAS^{G12D}$ protein without histidine tag was concentrated and flash frozen. Purity was checked by SDS-PAGE gel. For biochemical studies, $KRAS^{G12D}$ construct was expressed in *Escherichia coli* BL21-Gold (DE3) cells (Stratagene) growing at 37 °C in LB media with 100 μg/mL ampicillin and induced when the OD_{600nm} reached 1.0, with 1 mM isopropyl β-D-thiogalactoside at 15 °C overnight. Protein purification was the same as for the ^{15}N-labeled protein, except the N-terminal His_6 tag was not removed.

^1H-^{15}N HSQC experiments were performed on Bruker Avance III 500 (500 MHz) and Avance III 500 Ascend (500 MHz) spectrometers (Columbia University) at 298 K. Uniformly ^{15}N-labeled $KRAS^{G12D}$ was dissolved at 50 μM in NMR Buffer (50 mM HEPES pH 7.4, 50 mM NaCl, 2 mM $MgCl_2$, 2 mM TCEP, and 10% D_2O). The ^1H carrier frequency was positioned at the water resonance. The ^{15}N carrier frequency was positioned at 115 ppm. The spectral width in the ^1H dimension was 8,012 Hz, and the width in ω_2 (^{15}N) dimension was 4,054 Hz. Suppression of the water signal was accomplished using the WATERGATE sequence. Heteronuclear decoupling was accomplished using the GARP decoupling scheme. Assignments of wild-type KRAS loaded with GDP were previously published (Vo et al., 2013). We used the conditions reported to efficiently transfer the assignments to the peaks of our ^1H-^{15}N HSQC spectrum of the $KRAS^{G12D}$-GDP protein. To verify assignments, we performed 3D-^1H-^{15}N-^1H-NOESY-HSQC and 3D-^1H-^{15}N-^1H-TOCSY-HSQC experiments on $KRAS^{G12D}$. The 3D NMR experiments were performed on Bruker Avance US^2 800 (800 MHz) and Bruker Avance III 600 (600 MHz) spectrometers equipped with 5-mm TXI cryogenic probes (New York Structural Biology Center). The ^{15}N-NOESY-HSQC and ^{15}N-TOCSY-HSQC spectra were recorded at 298 K on uniformly ^{15}N-labeled $KRAS^{G12D}$ at 500 μM in NMR Buffer. The ^1H carrier frequency was positioned at the water resonance. The ^{15}N carrier frequency was positioned at 117 ppm. The spectral width in the ^1H dimension was 8,402 Hz, the width in ω_2 (^{15}N) dimension was 2,554 Hz, and the width in ω_3 was 8,389 Hz. The ^{15}N-NOESY-HSQC was recorded with a mixing time of 150 ms. The ^{15}N-TOCSY-HSQC spectra were recorded using DIPSI-2 mixing time of 70 ms. The TOCSY-HSQC spectrum was recorded with gradient enhancement. All data were processed and analyzed using TopSpin 3.1 (Bruker) and Sparky (Developed by T. D. Goddard and D. G. Kneller, UCSF). The mean chemical shift difference for ^1H and ^{15}N ($\Delta\delta_{NH}$) was calculated using:

$$\Delta\delta_{NH}=\frac{\sqrt{(\Delta\,\delta H_N)^2+((\frac{\Delta\delta N}{10}))^2}}{2}$$

Protein crystallization—In attempts to elucidate the binding mode of the compound to oncogenic KRAS, we crystallized the G12D mutant in complex with Mg-GDP or Mg-GDPNP, as well as the G12V mutant in complex with Mg-GDP, and collected X-ray diffraction data at 1.83, 1.95, and 1.5 Å resolution, respectively (Table S1). However, no electron density was observed for the compound after extensive efforts, including both co-crystallization and soaking experiments. The overall structures of the protein and the detailed binding modes of the guanine nucleotide are similar to those reported previously. For structural studies, $KRAS^{G12D}$ construct was expressed in *Escherichia coli* BL21-Gold (DE3) cells growing at 37°C in LB media with 100 μg/mL ampicillin and induced when OD_{600nm} reached 1.0, with 1 mM isopropyl β-D-thiogalactoside at 15°C overnight. Cells were pelleted and lysed by sonication in lysis buffer containing 10 mM Tris-HCl, 500 mM NaCl, 5 mM imidazole, 5 mM $MgCl_2$, pH 7.5, 0.5 % CHAPS (w/v), 1 mM TCEP and complete EDTA-free protease inhibitor tablets (Roche). Cell lysate was then centrifuged at 15,000 x *g* for 45 min at 4°C and loaded onto a chromatography column packed with Ni Sepharose 6 Fast Flow beads (GE Life Sciences) in buffer containing 10 mM Tris-HCl, 500 mM NaCl, 5 mM imidazole, 5 mM $MgCl_2$, pH 7.5, and 1mM TCEP. $KRAS^{G12D}$ was eluted with 250 mM imidazole in the same buffer. The eluted $KRAS^{G12D}$ was further purified using gel filtration Superdex 100 column in FPLC buffer (25 mM Tris-HCl pH 8, 100 mM NaCl, 5 mM $MgCl_2$, and 1 mM TCEP). The fractions containing $KRAS^{G12D}$ were pooled together and verified by SDS-PAGE. Protein concentration was determined using absorbance at 280 nm with extinction coefficient of 11,920 M^{-1} cm^{-1}. To generate the GppNHp-protein crystals, $KRAS^{G12D}$ was treated with ten molar excess of EDTA for 1 h at room temperature and then buffer exchanged into buffer B (25 mM Tris-HCl pH 8, 100 mM NaCl, 0.1 mM $ZnCl_2$, 5 mM $MgCl_2$, 1mM TCEP), supplemented with 10 mM GppNHp and treated with 250 UN alkaline phosphatase on agar beads (Sigma-Aldrich, cat P0762) for 18 h at 4 °C. The next day, the alkaline phosphatase beads were removed and $KRAS^{G12D}$ dialyzed into FPLC buffer. Diffraction quality crystals were grown at 20 °C from 0.5 + 0.5 μL sitting drops for vapor diffusion. For the G12V-Mg-GDP crystal, the drop contained 70 mg/mL $KRAS^{G12V}$ in 0.1M Bis-Tris pH 6.5, 25% w/v PEG3350. For the G12D-Mg-GppNHp crystal, the drop contained 70 mg/mL $KRAS^{G12D}$ in 0.1M Bis-Tris pH 5.5, 25% w/v PEG3350. For the G12D-Mg-GDP crystal, the drop contained 100 mg/mL $KRAS^{G12D}$, 10 mM small-molecule ligand, 4% DMSO, in 0.2 M sodium phosphate dibasic dihydrate, 20% w/v PEG 3350, pH 9.1 reservoir buffer. X-ray diffraction data for G12V-Mg-GDP and G12D-Mg-GppNHp were collected at 100 K at the X29 beamline of the National Synchrotron Light Source, and the X-ray diffraction data for G12D-Mg-GDP were collected using a Saturn 944HG charge-coupled device (CCD) detector mounted on a Rigaku MicroMax-003 microfocus X-ray generator. The diffraction images were processed with the program HKL2000 (Otwinowski and Minor, 1997). The structures were determined by the molecular replacement method with the program Phaser (McCoy et al., 2007), and refined with the programs Refmac (Murshudov et al., 1997) and PHENIX (Adams et al., 2002).

Twinned refinement was used for the G12V-Mg-GDP structure. The crystallographic statistics are summarized in Table S1.

In vitro RAS pulldown assay—A 20 μM solution of $KRAS^{G12D}$ in 50 mM HEPES, 200 mM sodium chloride, 2 mM TCEP with 1 mM EDTA and 1 mM GTP was gently rotated at 25 °C to remove the endogenous nucleotide. Magnesium chloride was then added to 5 mM and the resulting solution was rotated at 4°C for 4 h. The GTP-loaded $KRAS^{G12D}$ was then diluted to 20 nM and incubated with the inhibitors and 10 μL of RAF1-RBD agarose beads (EMD Millipore, CN: 14-278) or 100 nM recombinant GST-tagged human RALGDS protein (Abcam, CN: ab132590) with 20 μL of glutathione beads for 2 h. The beads were separated from solution by centrifuging at 1,500 × *g*. They were then washed twice with PBS before the addition of 1X SDS buffer. The quantity of RAS in the samples was then analyzed using the western blotting procedure.

Determining RAS isoform dependency using siRNAs—Small interfering RNAs (siRNAs) targeting each RAS isoform were purchased from Dharmacon Technologies. siRNA Catalog numbers:

siDEATH: AllStars Hs Cell Death Control siRNA; Cat # 1027299 from QIAGEN

siHRAS: ON-TARGETplus SMARTpool human HRAS siRNA; Cat # L-004142-00-0005 from GE Dharmacon

siKRAS: ON-TARGETplus SMARTpool human KRAS siRNA; Cat # L-005069-00-0010 from GE Dharmacon

siNRAS: ON-TARGETplus SMARTpool human NRAS siRNA; Cat # L-003919-00-0005 from GE Dharmacon

siNonTargetting: ON-TARGETplus Non-targeting Pool siRNA; Cat # D-001810-10-20 from GE Dharmacon

Reverse transfection was performed by preparing a solutions of 1 mL of Opti-MEM (Invitrogen) with 6 μL of Lipofectamine RNAiMAX (Invitrogen) and 5 μL of RNAi solution (10 μM stock), and by incubating the mixture (1 mL/well) in a 6-well plate for 30 min at 37°C. While the siRNA complex was forming, 0.2 million cells were suspended in 1 mL of 2X serum-containing media. The cell solution (1 mL) was transferred to each well of the 6-well plate containing siRNA complex (1 mL), and the 6-well plate was returned to the culture incubator. At 24, 48, 72 and 96 h post transfection cells were trypsinized and viability was determined using Trypan blue exclusion assay.

Confirming RAS knockdown using RT-qPCR experiment—Cells were detached from the 6-well plate, and 0.5 million cells were collected as a pellet by centrifuging 1,000 rpm for 5 min. Total cellular RNA sample was prepared using RNAeasy extraction kits (QIAgen) according to manufacturer's instruction. The resulting RNA sample was reverse-transcribed using a High Capacity cDNA Reverse Transcription kit (Life Technologies). The cDNA samples were mixed with TaqMan® probes for each *RAS* isoform gene, and arrayed on 96-well plate in triplicates. The plate was loaded onto viiA7 Real-Time PCR system (Life

Technologies) for qPCR reaction. Comparative analysis (ΔΔCt analysis) was performed with ACTB (human actin b), an internal reference gene.

Gene expression analysis by RT-qPCR—Cells from six-well plates were trypsinized and centrifuged at 3,000 rpm for 3 min. The cell pellet was then lysed and the RNA was extracted using the QIAshredder and RNAeasy extraction kits (Qiagen) according to the manufacturer's protocol. 2 μg of RNA from each sample was then converted to cDNA using the TaqMan RT Kit (Applied Biosystems). Primers for Quantitative PCR (qPCR) were designed with Primer Express. qPCR was performed using Power SYBR Green Master Mix (Applied Biosystems) in a 96-well format, in triplicate, using an Applied Biosystems 7300 Cycler set to absolute internal reference gene.

RAS, PI3K and BRAF overexpression—Phoenix-AMPHO (ATCC: CRL-3213) cells were seeded in a 6-well plate at 600,000 cells/well in 10% FBS and 1% P/S in DMEM 24 h prior to use. A solution of Lipofectamine 2000 (6 μL) in 100 μL Opti-mem media (reduced serum media) and the plasmid (2.5 μg) in 100 μL Opti-mem media were combined and incubated 5 min at 25 °C, then added to 1.8 mL of Opti-mem in each well. After 12 h, the medium was replaced with 10% FBS and 1% P/S in DMEM. The next day the supernatant was collected three times spaced 4 h apart and polybrene was added (1/1000). The supernatant was filtered (0.45 μm) and added to HT-1080 cells seeded at 100,000 cells per well (6-well dish) in 2 mL portions spaced 4 h apart. After 48 h, the cells were trypsinized and re-seeded in medium containing puromycin (2 μg/mL). After 6 d of selection, the cells were analyzed for expression using the qPCR procedure. 2 mL solutions of the inhibitors were added to a 6-well plate of the transfected HT-1080 cells (100,000 cells/well) and treated for 24 h. The cells were then trypsinized, re-suspended in 1 mL of medium and viability was measured by Vi-Cell (Beckman Coulter) through mixing with Trypan blue. pBABE-puro was from Addgene (plasmid # 1764). pBABE puro KRAS G12V was from Addgene (plasmid # 9052). pBabe-Puro-BRAF-V600E was from Addgene (plasmid # 15269). pBabe puro HA PIK3CA E545K was from Addgene (plasmid # 12525). pBABEbleo-Flag-BRAFV600E was from Addgene (plasmid # 53156).

Multicellular tumor spheroids—Multicellular tumor spheroids (MCTSs) were grown in 96-well Corningware Ultra Low Attachment (ULA) Plates (CLS 3474). 100 μL of cell suspension containing 2 X 10^4 cells/ml was added to each well of the ULA plate containing 100 μL of a 2X solution of the desired concentration of compounds. Cells were incubated at 37 °C, 5% CO_2 for 72 h to allow for MCTS formation. After 72 h, 50 uL of a 50% solution of Alamar blue and medium were added and incubated for 12 h prior to measurements on a Victor3 plate reader as previously above.

RALA activation assay—BJeLR cells were seeded 16 h prior to use in 2% FBS in DMEM. Medium was aspirated and replaced with medium containing 3144 (from a 10 mM DMSO stock). After 6 h, cells were washed 2X with ice-cold buffer (25 mM Tris, 100 mM NaCl, 1 mM TCEP, 5 mM $MgCl_2$, 0.1% Tween-20 and 1 protease inhibitor per 25 mL). Cells were scraped, pelleted at 13,000 rpm for 10 min at 4 °C, then passed through a 26 gauge needle several times. The solution was spun down a second time at 13,000 rpm for 15

min at 4 °C, to remove unlysed cell and debris. RALBP1 agarose beads (EMD Millipore) were then added to the lysate and the solution was rotated at 4 °C for 2 h. The solutions were spun down at 1,500 x *g* for 2 min and the supernatant was removed by syringe. The beads were washed twice with this process with buffer, then re-suspended in 2.5X SDS.

Immunoprecipitations—BJeLR cells were seeded 16 h prior to use in 10% FBS in DMEM. Medium was aspirated and replaced with medium containing 3144 (from a 10 mM DMSO stock). After 6 h cells were washed 2X with ice-cold buffer (25 mM tris, 100 mM NaCl, 1 mM TCEP, 5 mM $MgCl_2$, 0.1% Tween-20 and 1 protease inhibitor per 25 mL). Cells were scrapped, pelleted at 13,000 rpm for 10 min at 4 °C, then passed through a 26 gauge needle several times. The solution was spun down a second time at 13,000 rpm for 15 min at 4 °C, to remove unlysed cells and debris. HRAS antibody (Santa Cruz, SC-520) was then added to the lysate (1:100) and the solution was rocked at 4 °C for 16 h. Protein A agarose beads were then added and the solution was rotated at 4 °C for an additional 6 h. The solutions were spun down at 1,500 x *g* for 2 min and the supernatant was removed by syringe. The beads were washed 2X by this process with buffer, then re-suspended in 2.5X SDS.

Caspase 3/7 activation assay—HT-1080 cells were seeded into 384-well plates, 1,000 cells per well. After 16 h, compounds (as 50 mM stocks in DMSO) were arrayed in a dilution series in 384-well polypropylene plates. Compound solutions were transferred at a 1:5 dilution into the assay plates for a total volume of 40 μL. After 24 h, 8 μL of a 1:100 solution of rhodamine 110 bis-(N-CBZ-L-aspartyl-L-glutamyl-L-valyl-L-aspartic acid amide) to lysis buffer (APO-1, Promega) was added and the plate was wrapped in aluminum foil and incubated at room temperature for 16 h. Fluorescence intensity was then determined using a Victor3 plate reader (Perkin Elmer) with a 490 nm excitation filter and a 535 nm emission filter.

Mass Spectrometry Analysis of Nucleotide-Binding—Recombinant $KRAS^{G12D}$ with N-terminal His-tag with the following sequence was used in these experiments (calculated monoisotopic mass = 21322.59 Da):
GSSHHHHHHSSGLVPRGSHMTEYKLVVVGADGVGKSALTIQLIQNHFVDEYDPTIED
SYRKQVVIDGETCLLDILDTAGQEEYSAMRDQYMRTGEGFLCVFAINNTKSFEDIHH
YREQIKRVKDSEDVPMVLVGNKCDLPSRTVDTKQAQDLARSYGIPFIETSAKTRQGV
DDAFYTLVREIRKHKEK

Nucleotide exchange and sample preparation—Nucleotides in endogenous recombinant KRAS were exchanged with GDP, GTP or GppNHp using EDTA. Endogenous $KRAS^{G12D}$ protein (250 μM final) was incubated with 40-fold molar excess of EDTA (10 mM final), and 75-fold molar excess of new nucleotide (18.75 mM final) for 2 h at 30°C. After incubation, the sample was put on ice for 2 min and then $MgCl_2$ was added (65 mM final concentration) to stop the reaction. To remove excess unbound nucleotide, the sample was added to a NAP-5 column (GE Life Sciences) equilibrated with Buffer A (25 mM HEPES, 100 mM NaCl, 2 mM TCEP, pH 7.5) and eluted with Buffer A at three drops per fraction. Eluted fractions were examined using Bradford dye-binding method for the

presence of protein and those containing protein were concentrated, and buffer exchanged into water using Millipore spin column (13,900 x *g* for 7 min at 4°C, repeated six times, each time adding fresh MilliQ water and discarding the flow-through). Protein concentration was determined using absorbance at 280 nm with extinction coefficient of 11920 M^{-1} cm^{-1}. To check for success of nucleotide loading procedure, differential scanning fluorimetry was performed (see above). Protein sample in water was then diluted to 50 μM into a denaturing buffer (50% MeOH with 0.05% formic acid) or a native mode buffer (10 mM ammonium acetate) for mass spectrometry analysis.

Mass spectrometry—A 6 μL aliquot of each 50 μM protein solution was loaded into a fresh EconoTip Emitter, 1.2 mm OD with standard coating (New Objective, Woburn, MA). Emitters were mounted on a Nanospray Flex Ion Source fitted with a NanoES off-Line kit ES259, and spectra were collected on Orbitrap Q Exactive HF mass spectrometer (Thermo Fisher Scientific, Bremen, Germany). Direct infusion of sample into the instrument was effected without any applied hydrostatic pressure, but solely by the spray voltage of 1.5–1.7 kV in positive ion mode. Flow rate was estimated to be 20 – 80 nL/min. Heated capillary was set at 250°C and the S-Lens RF level was 55%. Scan range was 400 – 2000 m/z for samples added to 50% MeOH with 0.05% formic acid or 400 – 5000 m/z for samples in 10 mM ammonium acetate, resolution was 60,000, AGC target 1e6, and maximum inject time was 30 ms.

Protein Deconvolution—Mass spectra were processed in Qual Browser of Thermo Xcalibur (Thermo Scientific) to signal average spectra from 1–2 min into a single summed spectrum for each analysis. Spectra were analyzed using Thermo Scientific Protein Deconvolution software (Version 3.0.99.7). The DefaultMethodXtract under Manual Xtract (Isotopically Resolved) algorithm was used for deconvolution. Analysis parameters were set at m/z range 400 – 2000 m/z for samples in 50% MeOH with 0.05% formic acid or 400 – 5000 m/z for samples in 10 mM ammonium acetate. Charge carrier was set to H+, output mass to M, resolution at 400 m/z at 60,000, S/N threshold to 3, minimum detected charge to 3, and isotope table as protein. The deconvoluted results were exported to Microsoft Excel for further analysis. Theoretical modification and adduct masses are derived from Unimod (http://www.unimod.org) and Delta Mass https://abrf.org/delta-mass. Some ligand masses were found on the Chemical Entities of Biological Interest (ChEBI) website (https://www.ebi.ac.uk/chebi/. Raw mass spectrometry files have been deposited in an international data repository for proteomics https://chorusproject.org/ at the URL https://chorusproject.org/anonymous/download/experiment/3708034170230406717

Analysis of Mass Spectra—Spectra were successfully recorded for denatured samples in methanol and the native mode samples in ammonium acetate (see Table S4 and Supporting Information). Mean measured mass deviation from theoretical was +/− 0.04 Da for both native and denatured samples. Mean charge state was +23 for proteins under denaturing conditions and +11 for proteins under native mode conditions. Lower mean charge state observed in native mode suggested that the protein retained much of its secondary structure and consequently fewer charged groups were available to hold a charge. The apoprotein ($KRAS^{G12D}$) was the predominant species in all of the methanol

experiments (see Table S4 and Supporting Information), but none of the ammonium acetate experiments (see Table S4 and Supporting Information), suggesting that ammonium acetate under the conditions used was effective in retaining much of the native structure of the protein. However, even in methanol, the GDP ligand was retained at some level in the endogenous protein, in the protein exchanged with GDP and in the protein exchanged with GppNHp. GTP was retained at low levels by the protein in the GTP-exchanged sample. Both GDP and GppNHp were also retained at low levels in the GppNHp-exchanged sample in methanol. The results suggest that these nucleotides are bound with high affinity and survive, at least to some extent, denaturing conditions in methanol. For native mode spectra recorded in ammonium acetate, the endogenous protein appeared as a mixture of the GDP and GTP ligands. However, exchange was 100% effective for both GDP and GTP (Table S3). No contaminating GTP was detected in the GDP-exchanged samples, and no contaminating GDP was detected in the GTP-exchanged samples. In contrast, the GppNHp exchange resulted in a mixture of KRAS contained either the GppNHp or the GDP ligands. GTP, which started out as less abundant in the endogenous samples, was completely displaced by GppNHp.

Synthesis of chemical materials—All reactions were carried out under a nitrogen atmosphere under anhydrous conditions unless indicated otherwise. Anhydrous methylene chloride (DCM), tetrahydrofuran (THF) and N,N-dimethylformamide (DMF) were purchased from Sigma-Aldrich. Reactions were magnetically stirred and monitored by thin layer chromatography carried out by Merck pre-coated 0.25 mm silica plates containing a 254 nm fluorescence indicator. Flash chromatography was performed on a Teledyne combiflash companion automatic flash chromatography system. Preparative thin layer chromatography was performed on 1 mm. Proton nuclear magnetic resonance spectra (^{1}H NMR, 300 MHz, 400 MHz, 500 MHz) and proton decoupled carbon nuclear magnetic resonance spectra (^{13}C NMR, 100 MHz, 125 MHz) were obtained on a Bruker DPX 300, 400, or 500 MHz instruments in deuterochloroform ($CDCl_3$) with residual chloroform as internal standard. Other deuterated solvents that were used include d_4-MeOD and d_6-DMSO. Abbreviations: DIPEA = diisopropylethyl amine, DCE = 1,2-dichloroethane, EtOAc = ethyl acetate, HBTU = O-(Benzotriazol-1-yl)-N,N,N′,N′-tetramethyluronium hexafluorophosphate, HCl = hydrochloric acid, MeOH = methanol, $MgSO_4$= magnesium sulfate, $NaHCO_3$ = sodium bicarbonate, Na_2SO_4 = sodium sulfate, NH_4Cl = ammonium chloride, $Pd(PPh_3)_4$ = Tetrakis(triphenylphosphine)palladium(0), RT = room temperature, TFA = trifluoroacetic acid, THF = tetrahydrofuran. See also Table S2 for reagents and Method S1 Synthesis of Chemical Materials.

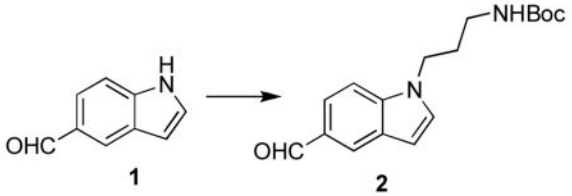

1 2

***tert*-butyl 3-(5-formyl-1*H*-indol-1-yl)propylcarbamate (2):** To a solution of 1*H*-indole-5-carbaldehyde (**1**) (2.72 g, 18.8 mmol) in DMF (80 mL) at 0 °C, sodium hydride (60% in

mineral oil) (0.69 g, 28.5 mmol, 1.5 equiv) was added in several portions over about 5 min. The mixture was stirred for 1 h at 0 °C before the sequential addition of 3-(Boc-amino)propyl bromide (8 g, 33.6 mmol). The solution was warmed to 80 °C and stirred for 48 h. Upon completion, the reaction was diluted with saturated aqueous $NaHCO_3$ and extracted three times with EtOAc. The combined organic layers were washed with brine, dried (Na_2SO_4), concentrated, and the crude material was purified by combiflash 0→50% EtOAc in hexanes to yield *tert*-butyl 3-(5-formyl-1*H*-indol-1-yl)propylcarbamate (**2**) (4.73 g, 83% yield). ^{1}H NMR (400 MHz, $CDCl_3$) δ 10.05 (s, 1H), 8.18 (d, *J* = 1.5 Hz, 1H), 7.81 (dd, *J* = 8.7, 1.6 Hz, 1H), 7.26 (d, *J* = 3.1 Hz, 1H), 6.75-6.60 (m, 1H), 4.54 (s, 1H), 4.25 (t, *J* = 6.9 Hz, 2H), 3.17 (d, *J* = 7.2 Hz, 2H), 2.08 (p, *J* = 6.9 Hz, 2H), 1.47 (s, 9H). ^{13}C NMR (100 MHz, $CDCl_3$) δ 192.4, 156.1, 139.2, 129.8, 129.3, 128.4, 126.6, 121.8, 109.8, 103.6, 79.5, 44.1, 38.0, 30.6, 28.4. HRMS (m/z): $[M]^+$ cald for $C_{17}H_{22}N_2O_3$, 302.1630, found 302.1633

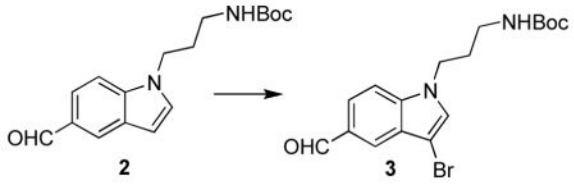

***tert*-butyl 3-(3-bromo-5-formyl-1*H*-indol-1-yl)propylcarbamate (3):** To a solution of *tert*-butyl 3-(5-formyl-1*H*-indol-1-yl)propylcarbamate (**2**) (4.73 g, 15.63 mmol) in dry THF (300 mL) at −78 °C, Br_2 (0.9 mL, 17.48 mmol, 1.1 equiv) was added dropwise over about 5 min. The resulting mixture was stirred at −78°C for 2.5 h. Upon completion, the reaction contents were poured onto a solution of ice (~300 g), water (200 mL), ammonium hydroxide (1 mL, 12 M), and sodium thiosultate pentahydrate (1 mL, saturated solution in water). The crude material was extracted three times with EtOAc, the combined organic layers were washed with brine, dried (Na_2SO_4), concentrated, and the crude material was purified by combiflash 0→50% EtOAc in hexanes to yield *tert*-butyl 3-(3-bromo-5-formyl-1*H*-indol-1-yl)propylcarbamate (**3**) (5.49 g, 92% yield).^{1}H NMR (400 MHz, $CDCl_3$) δ 10.09 (s, 1H), 8.12 (d, *J* = 1.5 Hz, 1H), 7.86 (dd, *J* = 8.7, 1.5 Hz, 1H), 7.43 (d, *J* = 8.6 Hz, 1H), 7.30 (s, 1H), 4.57 (s, 1H), 4.23 (t, *J* = 6.9 Hz, 2H), 3.18 (d, *J* = 6.8 Hz, 2H), 2.08 (p, *J* = 6.7 Hz, 2H), 1.47 (s, 9H). ^{13}C NMR (100 MHz, $CDCl_3$) δ 191.2, 155.3, 137.9, 129.0, 127.9, 126.5, 124.1, 121.6, 109.4, 91.2, 43.5, 37.1, 29.8, 27.6, 27.5. HRMS (m/z): $[M]^+$ cald for $C_{17}H_{21}BrN_2O_3$, 380.0736, found 380.0729.

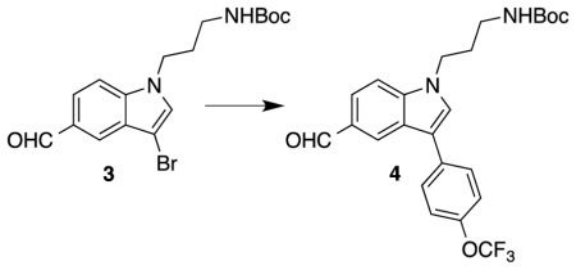

***tert*-butyl 3-(5-formyl-3-(4-(trifluoromethoxy)phenyl)-1*H*-indol-1-yl)propylcarbamate (4):** To a solution of *tert*-butyl 3-(3-bromo-5-formyl-1*H*-indol-1-yl)propylcarbamate (**3**)

(5.49 g, 14.39 mmol) in 1,4-dioxane (110 mL), 4-(trifluoromethoxy)phenylboronic acid (4.45 g, 21.59 mmol, 1.5 equiv), $Pd(PPh_3)_4$ (0.891 g, 0.77 mmol, 0.05 equiv), and a solution of potassium carbonate (14.4 mL, 2.0 M in H_2O) were added sequentially. The resulting mixture was heated to 100 °C in a thick walled high pressure sealed flask and stirred for 16 h. Upon completion, the reaction was cooled to rt and diluted with saturated aqueous $NaHCO_3$ and extracted three times with EtOAc. The combined organic layers were dried (Na_2SO_4), concentrated, and the crude material was purified by combiflash 0→40% EtOAc in hexanes to yield *tert*-butyl 3-(5-formyl-3-(4-(trifluoromethoxy)phenyl)-1*H*-indol-1-yl)propylcarbamate (**4**) (5.52 g, 84%). ^{1}H NMR (500 MHz, $CDCl_3$) δ 10.03 (s, 1H), 8.35 (s, 1H), 7.81 (d, *J* = 8.6 Hz, 1H), 7.64 (d,*J* = 8.4 Hz, 2H), 7.44 (d, *J* = 8.6 Hz, 1H), 7.40 (brs, 1H), 7.30 (d, *J* = 8.4 Hz, 2H), 4.25 (t, *J* = 6.9 Hz, 2H), 3.20-3.16 (m, 2H), 2.08 (p, *J* = 6.8 Hz, 2H), 1.43 (s, 9H). ^{13}C NMR δ (125 MHz, $CDCl_3$) 192.3, 156.2, 147.9, 140.0, 133.3, 130.0, 128.8, 127.5, 126.2, 125.1, 122.7, 121.6, 117.9, 110.3, 79.7, 44.3, 38.1, 30.7, 28.4. HRMS (m/z): $[M+H]^+$ cald for $C_{24}H_{26}F_3N_2O_4$, 463.1845, found 463.1848.

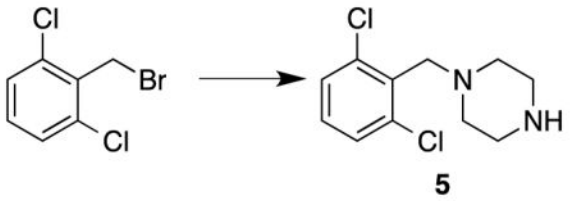

1-(2,6-dichlorobenzyl)piperazine (5): To a solution of piperazine (9.66 g, 112.1 mmol) in THF (180 mL) at 0 °C, a solution of 2,6-dichlorobenzyl bromide (4.52 g, 18.8 mmol) in THF (20 mL) was added dropwise over 10 min. The resulting mixture was slowly allowed to warm to RT and stirred for 24 h. Upon completion, the THF was removed, the crude material was re-suspended in CH_2Cl_2 and water, and extracted two additional times with CH_2Cl_2. The combined organic layers were dried (Na_2SO_4), filtered, and concentrated. The crude material was purified by combiflash 0→20% MeOH in CH_2Cl_2 to provide 1-(2,6-dichlorobenzyl)piperazine (**5**) (4.1 g, 88% yield). ^{1}H NMR (500 MHz, d_4-MeOD) δ 7.37 (d, *J* = 8.2 Hz, 2H), 7.24 (dd, *J* = 8.4, 8.3 Hz, 1H), 3.76 (s, 2H), 2.82 (dd, *J* = 5.0, 4.9 Hz, 4H), 2.59 (dd, J = 5.0, 4.9 Hz, 4H). ^{13}C NMR (125 MHz, d_4-MeOD) δ 138.1, 135.0, 130.6, 129.6, 57.8, 54.4, 46.2. HRMS (m/z): $[M+H]^+$ cald for $C_{11}H_{15}N_2Cl_2$, 245.0612, found 245.0607.

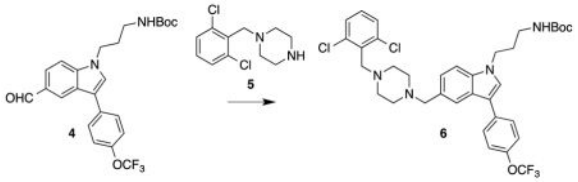

***tert*-butyl 3-(5-((4-(2,6-dichlorobenzyl)piperazin-1-yl)methyl)-3-(4-(trifluoromethoxy)phenyl)-1*H*-indol-1-yl)propylcarbamate (6):** To a solution of *tert*-butyl 3-(5-formyl-3-(4-(trifluoromethoxy)phenyl)-1*H*-indol-1-yl)propylcarbamate (**4**) (324.4 mg, 0.7 mmol) and 1-(2,6-dichlorobenzyl)piperazine (**5**) (267.4 mg, 1.1 mmol) in CH_2Cl_2 (4.5 mL) was added sodium triacetoxyborohydride (442.5 mg, 2.1 mmol). The resulting mixture

was stirred at 25 °C for 6 h. Upon completion, the reaction was diluted with water and extracted three times with CH_2Cl_2. The combined organic layers were dried (Na_2SO_4), concentrated, and the crude material was purified by combiflash 0→5% MeOH in DCM to yield *tert*-butyl 3-(5-((4-(2,6-dichlorobenzyl)piperazin-1-yl)methyl)-3-(4-(trifluoromethoxy)phenyl)-1*H*-indol-1-yl)propylcarbamate (454.5 mg, 94% yield). ^{1}H NMR (400 MHz, d_4-MeOD) δ 7.93 (d, *J* = 1.0 Hz, 1H), 7.72 (d, *J* = 8.7 Hz, 2H), 7.54 (s, 1H), 7.45 (d, *J* = 8.5 Hz, 1H), 7.32 (d, *J* = 8.1 Hz, 2H), 7.30 (d, *J* = 8.8 Hz, 2H), 7.23 (dd, *J* = 8.5, 1.2 Hz, 1H), 7.20 (dd, *J* = 8.6, 7.5 Hz, 1H), 4.22 (t, J = 6.9 Hz, 2H), 4.01 (s, 2H), 3.75 (s, 2H), 3.05 (t, *J* = 6.6 Hz, 2H), 2.86 brs, 4H), 2.69 (brs, 4H), 1.99 (p, J = 6.8 Hz, 2H), 1.42 (s, 9H). ^{13}C NMR (125 MHz, d_4-MeOD) δ 178.1, 158.5, 148.4, 138.4, 138.0, 136.0, 134.5, 130.8, 129.6, 129.5, 128.7, 127.5, 125.6, 123.2, 122.5, 116.5, 111.3, 80.0, 62.9, 56.7, 53.0, 51.7, 44.8, 38.8, 31.3, 28.8, 22.9. HRMS (m/z): $[M+H]^+$ cald for $C_{35}H_{40}Cl_2F_3N_4O_3$, 691.2430, found 691.2449.

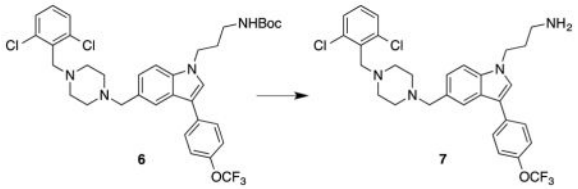

3-(5-((4-(2,6-dichlorobenzyl)piperazin-1-yl)methyl)-3-(4-(trifluoromethoxy)phenyl)-1*H*-indol-1-yl)propan-1-amine (7): To a solution of *tert*-butyl 3-(5-((4-(2,6-dichlorobenzyl)piperazin-1-yl)methyl)-3-(4-(trifluoromethoxy)phenyl)-1*H*-indol-1-yl)propylcarbamate (**6**) (1.88 g, 2.72 mmol) in 1,4-dioxane (50 mL) a solution of HCl (20 mL, 4.0 M in 1,4-dioxane) was added and the resulting solution was stirred at 25 °C for 16 h. Upon completion, the 1,4-dioxane was removed and the crude material was re-suspended in methanol and an excess of potassium carbonate was added. The slurry was stirred at RT until basic, filtered over celite and concentrated. The crude product was purified by preparative TLC (20% MeOH in CH_2Cl_2) to provide 3-(5-((4-(2,6-dichlorobenzyl)piperazin-1-yl)methyl)-3-(4-(trifluoromethoxy)phenyl)-1*H*-indol-1-yl)propan-1-amine (**7**) (1.61 g, 100% yield).

^{1}H NMR (400 MHz, d_4-MeOD) δ 7.80 (s, 1H), 7.71 (d, *J* = 8.5 Hz, 2H), 7.50 (s, 1H), 7.41 (d, *J* = 8.4 Hz, 1H), 7.30 (dd, J = 8.2, 8.2 Hz, 4H), 7.19-7.15 (m, 2H), 4.26 (t, *J* = 6.8 Hz, 2H), 3.70 (s, 2H), 3.56 (s, 2H), 2.71 (t, *J* = 7.1 Hz, 2H), 2.57 (brs, 4H), 2.43 (brs, 4H), 2.05 (p, *J* = 7.1 Hz, 2H). ^{13}C NMR (125 MHz, d_4-MeOD) δ 148.3, 138.1, 137.8, 136.4, 135.1, 130.5, 129.64, 129.56, 129.3, 127.8, 127.3, 125.4, 122.4, 121.9, 121.0, 116.4, 110.7, 64.5, 57.2, 53.9, 53.7, 44.7, 39.4, 32.7. HRMS (m/z): $[M+H]^+$ cald for $C_{30}H_{32}Cl_2F_3N_4O$, 591.1900, found 591.1906

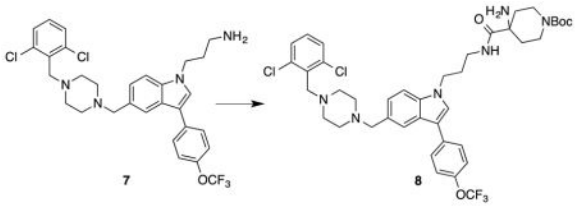

<u>*tert*-butyl 4-amino-4-(3-(5-((4-(2,6-dichlorobenzyl)piperazin-1-yl)methyl)-3-(4-(trifluoromethoxy)phenyl)-1*H*-indol-1-yl)propylcarbamoyl)piperidine-1-carboxylate (8):</u> HBTU (1.22 g, 5.43 mmol) was added to a solution of 4-amino-1-(*tert*-butoxycarbonyl)piperidine-4-carboxylic acid (0.99 g, 4.05 mmol) and DIPEA (0.70 mL, 4.01 mmol) in dry DMF (25 mL) at 0 °C and stirred for 1 h. A solution of 3-(5-((4-(2,6-dichlorobenzyl)piperazin-1-yl)methyl)-3-(4-(trifluoromethoxy)phenyl)-1*H*-indol-1-yl)propan-1-amine (**7**) (1.6 g, 2.70 mmol) in dry DMF (10 mL) was added. The reaction was stirred for an additional 48 h and allowed to warm to 25 °C. Upon completion, the reaction was quenched with saturated aqueous $NaHCO_3$ and extracted three times with EtOAc. The combined organic layers were washed with water and brine, dried (Na_2SO_4), filtered and concentrated. The crude material was purified by combiflash 0→5% MeOH in CH_2Cl_2 to yield *tert*-butyl 4-amino-4-(3-(5-((4-(2,6-dichlorobenzyl)piperazin-1-yl)methyl)-3-(4-(trifluoromethoxy)phenyl)-1*H*-indol-1-yl)propylcarbamoyl)piperidine-1-carboxylate (**8**) (1.59 g, 72% yield). ^{1}H NMR (400 MHz, $CDCl_3$) δ 7.75 (s, 1H), 7.62 (d, *J* = 8.7 Hz, 3H), 7.33-7.28 (m, 6H), 7.11 (t, *J* = 8.0 Hz, 1H), 4.21 (t, *J* = 6.6 Hz, 2H), 3.90 (brd, *J* = 11.6 Hz, 2H), 3.75 (s, 2H), 3.68 (s, 2H), 3.30 (q, *J* = 6.5 Hz, 2H), 2.94 (m, 2H), 2.80 (m, 3H), 2.63 (brs, 4H), 2.54 (brs, 4H), 2.14-2.01 (m, 5H), 1.45 (s, 9H), 1.18 (brd, *J* = 13.6 Hz, 1H). ^{13}C NMR (100 MHz, $CDCl_3$) δ176.9, 154.7, 147.4, 137.1, 136.2, 134.4, 134.3, 128.9 128.5, 128.4, 126.2, 124.4, 121.7, 121.6, 120.8, 119.7, 115.8, 109.7, 79.8, 63.5, 56.4, 55.5, 53.1, 52.7, 44.7, 38.7, 37.2, 34.6, 30.1, 28.5. HRMS (m/z): $[M+H]^+$ cald for $C_{41}H_{50}Cl_2F_3N_6O_4$, 817.3223, found 817.3185

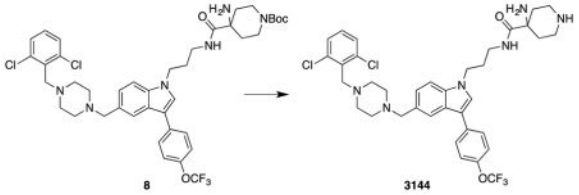

<u>4-amino-*N*-(3-(5-((4-(2,6-dichlorobenzyl)piperazin-1-yl)methyl)-3-(4-(trifluoromethoxy)phenyl)-1*H*-indol-1-yl)propyl)piperidine-4-carboxamide: 3144:</u> *tert*-butyl-4-amino-4-(3-(5-((4-(2,6-dichlorobenzyl)piperazin-1-yl)methyl)-3-(4-(trifluoromethoxy)phenyl)-1*H*-indol-1-yl)propylcarbamoyl)piperidine-1-carboxylate (**8**) (40 mg, 0.049 mmol) was dissolved in 1,4-dioxane (0.5 mL) before the addition of HCl in 1,4-dioxane (0.1 mL of a 4.0 M solution). The resulting mixture was stirred for 6 h at 25 °C. Upon completion the 1,4-dioxane was removed and the residue was re-suspended in MeOH and solid K_2CO_3 (100 mg, XS) was added. The crude material was purified by preparative TLC (15% MeOH in DCM) to provide 3144 (18 mg, 51%). ^{1}H NMR (400 MHz, d_4-MeOD) δ 7.82 (s, 1H), 7.74 (d, *J* = 8.7 Hz, 2H), 7.55 (s, 1H), 7.42 (d, *J* = 8.4 Hz, 1H), 7.34 (d, *J* =

8.0 Hz, 2H), 7.31 (d, *J* = 8.2 Hz, 2H), 7.21 (dd, J = 8.5, 7.5 Hz, 2H), 4.26 (t, *J* = 6.7 Hz, 2H), 3.75 (s, 2H), 3.60 (s, 2H), 3.24 (t, *J* = 6.6 Hz, 2H), 2.99-2.89 (m, 4H), 2.60 (brs, 4H), 2.49 (brs, 4H), 2.11-1.97 (m, 4H), 1.35 (brd, *J* = 13.9 Hz, 2H). ^{13}C NMR (100 MHz, d_4-MeOD) δ 179.4, 148.3, 138.1, 137.8, 136.4, 135.1, 130.5, 129.7, 129.6, 128.1, 127.4, 125.4, 122.5, 121.9, 116.3, 110.8, 64.5, 57.2, 56.2, 53.9, 53.7, 49.8, 45.2, 41.8, 38.3, 34.8, 30.8. HRMS (m/z): $[M+H]^+$ cald for $C_{36}H_{42}Cl_2F_3N_6O_2$, 717.2698, found 717.2675

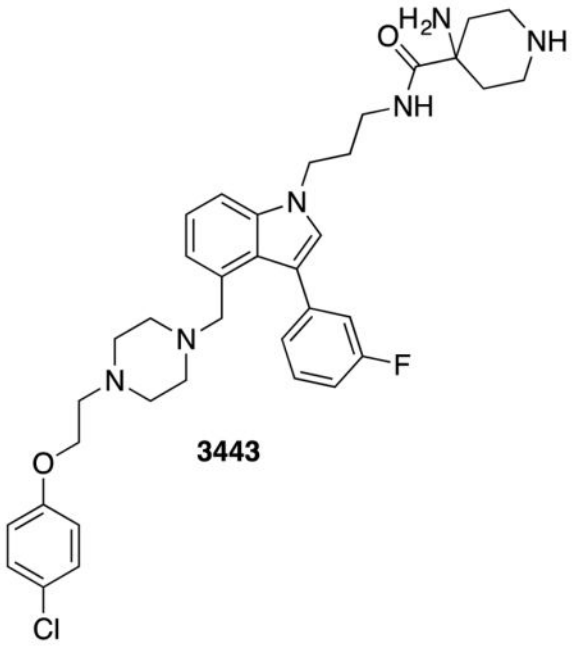

3443

4-amino-*N*-(3-(4-((4-(2-(4-chlorophenoxy)ethyl)piperazin-1-yl)methyl)-3-(3-fluorophenyl)-1*H*-indol-1-yl)propyl)piperidine-4-carboxamide: 3443: The compound prepared according to the protocols for 3144. ^{1}H NMR (400 MHz, d_4-MeOD) δ 7.44 (dd, *J* = 8.4, 1.0 Hz, 1H), 7.38 (td, *J* = 8.0, 6.1 Hz, 1H), 7.34-7.22 (m, 5H), 7.22-7.15 (m, 1H), 7.08-6.98 (m, 2H), 6.94-6.87 (m, 2H), 4.34-4.21 (m, 2H), 4.06 (t, *J* = 5.5 Hz, 2H), 3.56 (s, 2H), 2.73 (t, *J* = 5.5 Hz, 2H), 2.43 (s, 3H), 2.25-2.08 (m, 7H). ^{13}C NMR (100 MHz, *d*-MeOD) δ_4 177.3, 163.6, 161.1, 136.9, 128.9, 127.8, 126.2, 125.4, 122.2, 121.1, 117.0, 116.8, 115.7, 112.6, 109.3, 59.5, 56.4, 53.7, 52.7, 51.3, 43.5, 39.7, 36.9, 31.1, 29.3. HRMS (m/z): $[M+H]^+$ cald for $C_{36}H_{45}ClFN_6O_2$, 647.3271, found 647.3400

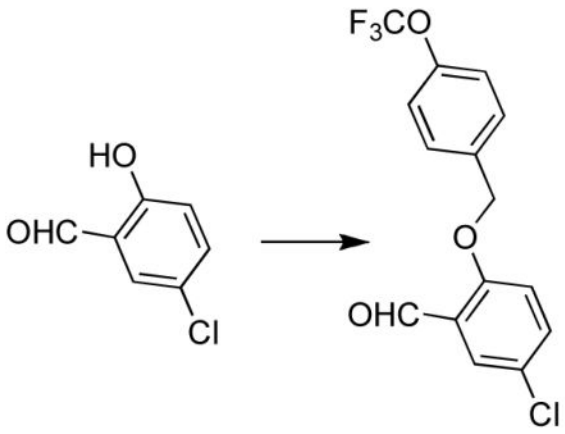

5-chloro-2-(4-(trifluoromethoxy)benzyloxy)benzaldehyde: To a solution of 5-chlorosalicyladehyde (82 mg, 0.56 mmol) in DMF (1 mL), K_2CO_3 (87 mg, 0.63 mmol) was added and stirred for 10 min at 25 °C before the addition of 4-(trifluoromethoxy)benzyl bromide (126 uL, 0.788 mmol). The resulting mixture was stirred at 25 °C for 12 h. Upon completion, the reaction contents were diluted with saturated $NaHCO_3$ and extracted with EtOAc (3X). The combined organic layers were washed once with brine, dried (Na_2SO_4), concentrated and purified by combiflash 0→ 30% EtOAc to provide 5-chloro-2-(4-(trifluoromethoxy)benzyloxy)benzaldehyde (99 mg, 53% yield). ^{1}H NMR (400 MHz, $CDCl_3$) δ 10.49 (s, 1H), 7.84 (d, J = 2.8 Hz, 1H), 7.55-7.45 (m, 3H), 7.34-7.23 (m, 2H), 7.01 (d, J = 8.9 Hz, 1H), 5.20 (s, 2H). ^{13}C NMR (100 MHz, $CDCl_3$) δ 188.1, 135.4, 134.23, 128.8, 128.3, 126.1, 121.3, 114.5, 70.04. HRMS (m/z): $[M-H]^+$ cald for $C_{15}H_9ClF_3O_3$, 329.0187, found 329.0180

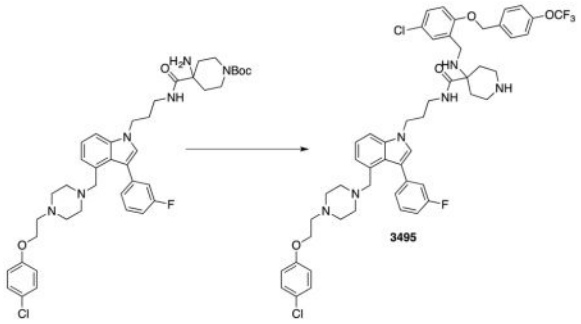

4-((5-chloro-2-((4-(trifluoromethoxy)benzyl)oxy)benzyl)amino)-*N*-(3-(4-((4-(2-(4-chlorophenoxy)ethyl)piperazin-1-yl)methyl)-3-(3-fluorophenyl)-1*H*-indol-1-yl)propyl)piperidine-4-carboxamide: 3495: To a solution of *tert*-butyl-4-amino-4-(3-(4-((4-(2-(4-chlorophenoxy)ethyl)piperazin-1-yl)methyl)-3-(3-fluorophenyl)-1*H*-indol-1-yl)propylcarbamoyl)piperidine-1-carboxylate (29 mg, 0.0443 mmol) in dichloroethane (1 mL), 5-chloro-2-(4-(trifluoromethoxy)benzyloxy)benzaldehyde (44 mg, 0.133 mmol), and $MgSO_4$ (10 mg) were added and stirred at 40 °C for 1 h prior to the addition of sodium triacetoxyborohydride (19 mg, 0.0886 mmol). The resulting mixture was stirred for an additional 8 h at 40 °C before being concentrated and purified directly by preparative TLC

(2% MeOH in DCM). The Boc group of the product was then removed (using the protocol for 3144) to provide compound 3495 (14 mg, 33% yield over two steps). ^{1}H NMR (400 MHz, d_4-MeOD) δ 7.41-7.29 (m, 5H), 7.29-7.13 (m, 8H), 7.12-6.97 (m, 4H), 6.92-6.86 (m, 2H), 5.71 (s, 1H), 4.95 (q, J = 11.1 Hz, 2H), 4.14 (q, J = 7.1 Hz, 2H), 4.05 (t, J = 5.5 Hz, 2H), 3.53 (s, 2H), 3.44 (ddd, J = 14.7, 9.1, 6.3 Hz, 1H), 3.16 (dtd, J = 27.2, 13.1, 11.7, 4.3 Hz, 3H), 3.00-2.80 (m, 2H), 2.72 (t, J = 5.5 Hz, 2H), 2.09-1.79 (m, 5H), 1.71 (d, J = 14.1 Hz, 1H). ^{13}C NMR (100 MHz, d_4-MeOD) δ 175.6, 157.5, 155.8, 136.8, 135.2, 130.4, 130.2, 129.7, 129.3, 128.9, 128.8, 128.7, 127.5, 126.2, 126.1, 126.0, 125.4, 125.3, 122.2, 121.1, 120.8, 117.0, 116.9, 116.7, 115.6, 114.0, 112.4, 112.2, 108.9, 69.5, 65.2, 59.7, 58.8, 56.7, 53.0, 51.8, 43.3, 40.5, 40.4, 38.4, 31.2, 29.7, 27.3. HRMS (m/z): $[M+H]^+$ cald for $C_{51}H_{55}Cl_2F_4N_6O_4$, 961.3592, found 961.3020

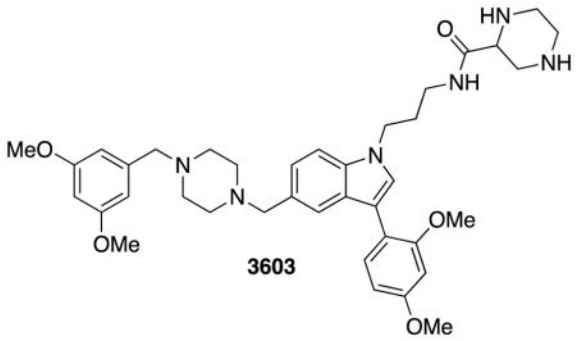

3603

***N*-(3-(5-((4-(3,5-dimethoxybenzyl)piperazin-1-yl)methyl)-3-(2,4-dimethoxyphenyl)-1*H*-indol-1-yl)propyl)piperazine-2-carboxamide: 3603:** 3603 was synthesized according to the analogous procedure as 3144.

^{1}H NMR (400 MHz, Methanol-d_4) δ 7.62 (s, 1H), 7.50 – 7.40 (m, 3H), 7.20 (d, J = 9.8 Hz, 1H), 6.68 (d, J = 2.5 Hz, 1H), 6.64 (dd, J = 8.3, 2.5 Hz, 1H), 6.52 (d, J = 2.3 Hz, 2H), 6.40 (t, J = 2.3 Hz, 1H), 4.55 (s, 3H), 4.29 (t, J = 6.8 Hz, 2H), 3.87 (s, 3H), 3.82 (s, 3H), 3.77 (s, 6H), 3.73 (s, 2H), 3.53 – 3.48 (m, 3H), 3.16 (p, J = 1.7 Hz, 1H), 2.77 – 2.48 (m, 11H), 2.36 (d, J = 7.5 Hz, 1H), 2.11 (t, J = 6.7 Hz, 2H), 0.95 – 0.84 (m, 4H).

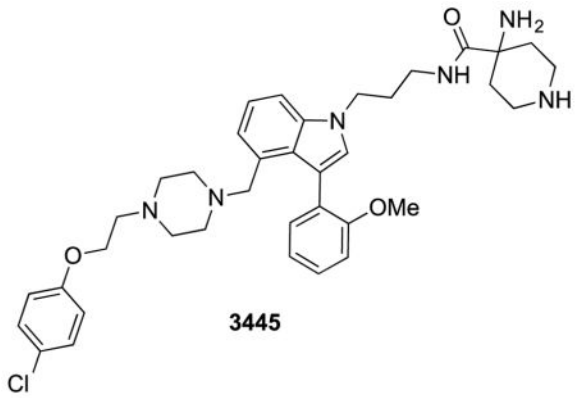

3445

4-amino-*N*-(3-(4-((4-(2-(4-chlorophenoxy)ethyl)piperazin-1-yl)methyl)-3-(2-methoxyphenyl)-1*H*-indol-1-yl)propyl)piperidine-4-carboxamide: 3445: 3445 was synthesized according to the analogous procedure as 3144.

^{1}H NMR (400 MHz, Methanol-d_4) δ 7.66 (d, J = 1.5 Hz, 1H), 7.58 (dd, J = 7.5, 1.7 Hz, 1H), 7.54 (s, 1H), 7.46 (d, J = 8.4 Hz, 1H), 7.32 – 7.20 (m, 4H), 7.11 (dd, J = 8.3, 1.1 Hz, 1H), 7.05 (td, J = 7.5, 1.2 Hz, 1H), 6.96 – 6.88 (m, 2H), 4.32 (t, J = 6.6 Hz, 2H), 4.12 (t, J = 5.5 Hz, 2H), 3.86 (s, 3H), 3.71 (s, 2H), 3.25 – 3.17 (m, 4H), 2.83 (t, J = 5.5 Hz, 2H), 2.66 (s, 7H), 2.20 – 2.07 (m, 4H), 1.49 (d, J = 14.4 Hz, 2H).

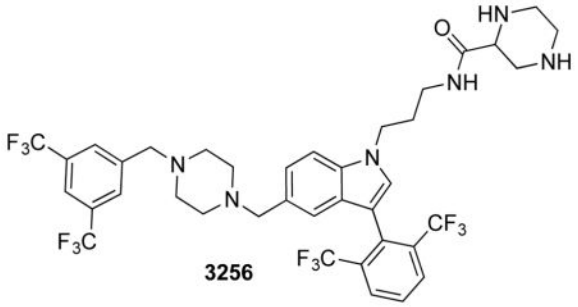

3256

***N*-(3-(5-((4-(3,5-bis(trifluoromethyl)benzyl)piperazin-1-yl)methyl)-3-(2,6-bis(trifluoromethyl)phenyl)-1*H*-indol-1-yl)propyl)piperazine-2-carboxamide: 3256:** 3256 was synthesized according to the same procedure as 3144.

^{1}H NMR (400 MHz, Methanol-d_4) δ 8.20 (d, J = 1.6 Hz, 2H), 7.94 (s, 2H), 7.87 (d, J = 13.8 Hz, 2H), 7.83 (s, 1H), 7.79 (s, 1H), 7.53 (d, J = 8.5 Hz, 1H), 7.30 (dd, J = 8.5, 1.5 Hz, 1H), 4.32 (t, J = 6.8 Hz, 2H), 3.84 (s, 2H), 3.71 (s, 2H), 3.58 – 3.45 (m, 1H), 3.36 – 3.33 (m, 2H), 3.28 – 3.17 (m, 2H), 3.11 – 3.00 (m, 2H), 2.97 – 2.81 (m, 3H), 2.72 (brs, 4H), 2.58 (brs, 4H), 2.12 (p, J = 6.6 Hz, 2H), 0.94 – 0.81 (m, 2H).

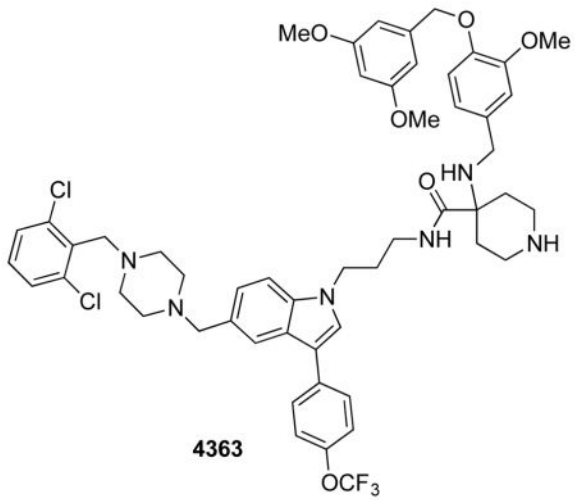

4363

***N*-(3-(5-((4-(2,6-dichlorobenzyl)piperazin-1-yl)methyl)-3-(4-(trifluoromethoxy)phenyl)-1*H*-indol-1-yl)propyl)-4-((4-((3,5-dimethoxybenzyl)oxy)-3-**

methoxybenzyl)amino)piperidine-4-carboxamide: 4363: 4363 was synthesized using the same procedures as 3495.

^{1}H NMR (400 MHz, Methanol-d_4) δ 7.84 (s, 1H), 7.74 (d, J = 8.7 Hz, 2H), 7.49 (s, 1H), 7.43 – 7.29 (m, 5H), 7.29 – 7.17 (m, 2H), 6.96 (s, 1H), 6.90 – 6.80 (m, 2H), 6.59 (d, J = 2.3 Hz, 2H), 6.40 (d, J = 2.4 Hz, 1H), 5.00 (s, 2H), 4.25 (t, J = 6.9 Hz, 2H), 3.81 (s, 3H), 3.79 (s, 2H), 3.75 (s, 6 H), 3.62 (s, 2H), 3.53 – 3.47 (m, 3H), 3.19 – 2.91 (m, 6H), 2.63 (s, 4H), 2.50 (s, 4H), 2.16 – 1.96 (m, 5H), 1.75 (d, J = 14.2 Hz, 2H).

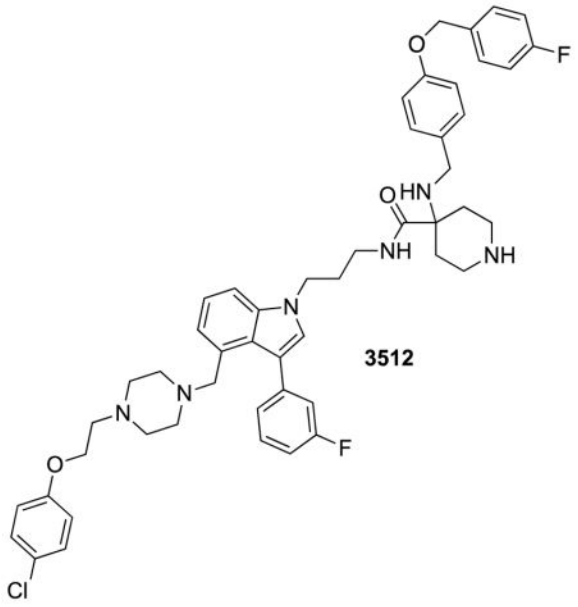

4-((3-chloro-4-((4-fluorobenzyl)oxy)benzyl)amino)-*N*-(3-(4-((4-(2-(4-chlorophenoxy)ethyl)piperazin-1-yl)methyl)-3-(3-fluorophenyl)-1*H*-indol-1-yl)propyl)piperidine-4-carboxamide: 3512: 3512 was synthesized according to the same procedures as 3495.^{1}H NMR (400 MHz, Methanol-d_4) δ 7.51 – 7.41 (m, 3H), 7.41 – 7.28 (m, 3H), 7.28 – 7.20 (m, 4H), 7.20 – 7.13 (m, 2H), 7.13 – 7.06 (m, 2H), 7.06 – 6.98 (m, 3H), 6.93 – 6.86 (m, 2H), 5.11 (s, 2H), 4.26 (t, J = 6.9 Hz, 2H), 4.06 (t, J = 5.5 Hz, 2H), 3.56 – 3.49 (m, 4H), 3.33 – 3.08 (m, 10H), 2.72 (t, J = 5.5 Hz, 2H), 2.41 (s, 3H), 2.12 (td, J = 15.9, 13.5, 7.6 Hz, 8H), 1.89 (d, J = 14.7 Hz, 2H).

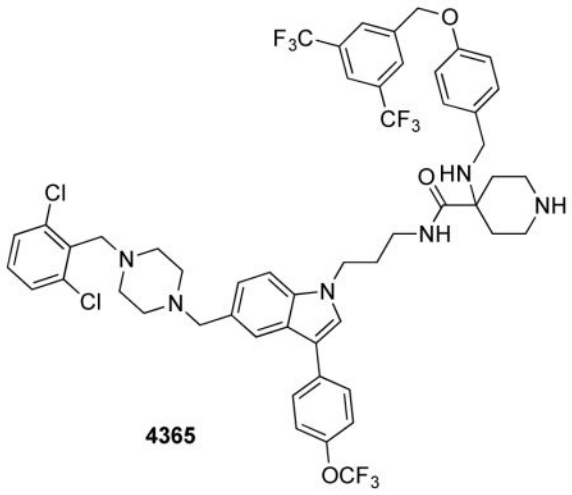

4365

4-((4-((3,5-bis(trifluoromethyl)benzyl)oxy)benzyl)amino)-*N*-(3-(5-((4-(2,6-dichlorobenzyl)piperazin-1-yl)methyl)-3-(4-(trifluoromethoxy)phenyl)-1*H*-indol-1-yl)propyl)piperidine-4-carboxamide: 4365: 4365 was synthesized using the same procedures as 3495.

^{1}H NMR (400 MHz, Methanol-d_4) δ 8.03 (s, 2H), 7.93 (s, 1H), 7.86 – 7.81 (m, 1H), 7.77 – 7.70 (m, 2H), 7.51 (s, 1H), 7.43 (d, J = 8.5 Hz, 1H), 7.40 – 7.34 (m, 2H), 7.26 (dddd, J = 23.7, 16.0, 8.2, 1.3 Hz, 7H), 7.00 – 6.93 (m, 2H), 5.20 (s, 2H), 4.27 (t, J = 6.8 Hz, 2H), 3.78 (s, 2H), 3.62 (s, 2H), 3.48 (s, 3H), 3.11 – 2.99 (m, 2H), 2.99 – 2.89 (m, 2H), 2.63 (s, 4H), 2.50 (s, 4H), 2.11 (t, J = 6.7 Hz, 2H), 1.99 (ddd, J = 13.9, 9.7, 4.0 Hz, 2H), 1.70 (d, J = 14.5 Hz, 2H).

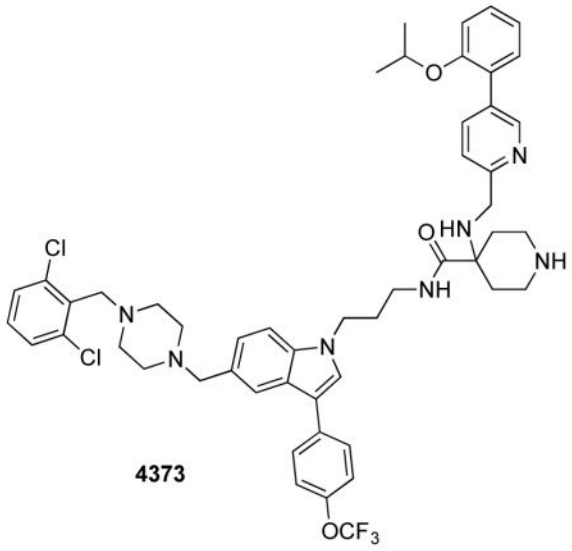

4373

***N*-(3-(5-((4-(2,6-dichlorobenzyl)piperazin-1-yl)methyl)-3-(4-(trifluoromethoxy)phenyl)-1*H*-indol-1-yl)propyl)-4-(((5-(2-isopropoxyphenyl)pyridin-2-**

yl)methyl)amino)piperidine-4-carboxamide: 4373: 4373 was synthesized using the same procedures as 3495.

^{1}H NMR (400 MHz, Methanol-d_4) δ 8.65 (d, J = 2.2 Hz, 1H), 7.91 (dd, J = 8.1, 2.2 Hz, 1H), 7.85 (s, 1H), 7.76 – 7.69 (m, 2H), 7.53 (s, 1H), 7.47 (d, J = 8.0 Hz, 1H), 7.42 – 7.33 (m, 4H), 7.33 – 7.22 (m, 4H), 7.21 – 6.99 (m, 4H), 4.59 (p, J = 6.3 Hz, 1H), 4.30 (t, J = 6.9 Hz, 2H), 3.79 (d, J = 7.6 Hz, 4H), 3.69 (s, 2H), 2.61 (d, J = 29.0 Hz, 8H), 2.28 – 2.08 (m, 4H), 1.94 (d, J = 15.8 Hz, 3H), 1.31 – 1.21 (m, 3H), 1.20 (d, J = 6.0 Hz, 5H).

QUANTIFICATION AND STATISTICAL ANALYSIS

All statistical analyses, potency determinations, and viability curves were produced using Prism 5.0c (GraphPad Software). Number of samples and statistical tests used are provided in the STAR Methods.

DATA AND SOFTWARE AVAILABILITY

PDB files of structures generated and docked pose of 3144 are provided as Supplementary Materials. Raw mass spectrometry files have been deposited in an international data repository for proteomics https://chorusproject.org/. The URL is: https://chorusproject.org/anonymous/download/experiment/3708034170230406717

KEY RESOURCES TABLE

REAGENT or RESOURCE	SOURCE	IDENTIFIER
Antibodies		
Phospho-p44/42 MAPK (Erk1/2) (Thr202/Tyr204) Antibody	Cell Signaling Technology	Cat. No. 9101S; RRID:AB_331646
p44/42 MAPK (Erk1/2) Antibody	Cell Signaling Technology	Cat. No. 9102S; RRID:AB_330744
Anti-Phospho-Akt (Ser473) (D9E) XP(R) Rabbit mAb antibody	Cell Signaling Technology	Cat. No. 4060S; RRID:AB_2315049
Anti-AKT antibody	Cell Signaling Technology	Cat. No. 9272S; RRID:AB_329827
Anti-panRAS antibody	Cell Signaling Technology	Cat. No. 3965S; RRID:AB_10695608
Anti-HRAS antibody	Santa Cruz	Cat. No. SC-520; RRID:AB_631670
Anti-RalA antibody	Cell Signaling Technology	Cat. No. 4799S; RRID:AB_10612771
Anti-PI3Kgamma antibody	Cell Signaling Technology	Cat. No. 5405S; RRID:AB_1904087
c-Raf Antibody	Cell Signaling Technology	Cat. No. #9422; RRID:AB_390808
Anti-cleaved caspase-3 antibody	Cell Signaling Technology	Cat. No. 9664; RRID:AB_2070042
Goat anti-rabbit antibody conjugated to an IRdye at 800CW	Li-COR Biosciences	Cat. No. 926-32211; RRID:AB_621843
Donkey anti-mouse antibody conjugated to an IRdye at 680RD	Li-COR Biosciences	Cat. No. 926-68072; RRID:AB_10953628
Biological Samples		
T-ALL patient samples	University of Padova (Italy)	N/A
Chemicals, Peptides, and Recombinant Proteins		
(*Z*)-4-hydroxytamoxifen (4OHT)	Sigma	Cat. No. H7904
Recombinant Human EGF	PeproTech	Cat. No. AF-100-15
MG-132	Sigma Aldrich	Cat. No. M7449
7-ethoxycoumarin	Sigma Aldrich	Cat. No. E1379
Guanosine 5′-diphosphate sodium salt, Type I, >=96%	Sigma Aldrich	Cat. No. G7127
Guanosine 5′-triphosphate sodium salt hydrate,>=95%	Sigma Aldrich	Cat. No. G8877
Guanosine 5′-[beta,gamma-imido]triphosphate trisodium salt hydrate	Sigma Aldrich	Cat. No. G0635
RALA protein	Abcam	Cat. No. ab102555
RHOA protein	Abcam	Cat. No. ab101594
RRAS2 Human 50ug	ProSpecBio	Cat. No. PRO-728
RRAS Human 10ug	ProSpecBio	Cat. No. PRO-808

REAGENT or RESOURCE	SOURCE	IDENTIFIER
RAP1A Human 10ug	ProSpecBio	Cat. No. PRO-848
H-Ras (wild-type) (human), (recombinant)	Enzo Life Sciences	Cat. No. BML-SE131-0100
Recombinant Human K-Ras 25ug	Cell Biolabs	Cat. No. STA-748
Recombinant GST-tagged human RALGDS protein	Abcam	Cat. No. ab132590
Methylene chloride	Fisher Scientific	Cat. No. D37-20
Tetrahydrofuran, anydrous, 1L	Sigma-Aldrich	Cat. No. 186562-1L
4-amino-N-(3-(5-((4-(2,6-dichlorobenzyl)piperazin-1-yl)methyl)-3-(4-(trifluoromethoxy)phenyl)-1H-indol-1-yl)propyl)piperidine-4-carboxamide (3144)	This study	N/A
tert-butyl 3-(5-formyl-1*H*-indol-1-yl)propylcarbamate (2)	This study	N/A
tert-butyl 3-(3-bromo-5-formyl-1*H*-indol-1-yl)propylcarbamate (3)	This study	N/A
tert-butyl 3-(5-formyl-3-(4-(trifluoromethoxy)phenyl)-1H-indol-1-yl)propylcarbamate (4)	This study	N/A
1-(2,6-dichlorobenzyl)piperazine (5)	This study	N/A
tert-butyl 3-(5-((4-(2,6-dichlorobenzyl)piperazin-1-yl)methyl)-3-(4-(trifluoromethoxy)phenyl)-1H-indol-1-yl)propylcarbamate (6)	This study	N/A
3-(5-((4-(2,6-dichlorobenzyl)piperazin-1-yl)methyl)-3-(4-(trifluoromethoxy)phenyl)-1H-indol-1-yl)propan-1-amine (7)	This study	N/A
tert-butyl 4-amino-4-(3-(5-((4-(2,6-dichlorobenzyl)piperazin-1-yl)methyl)-3-(4-(trifluoromethoxy)phenyl)-1H-indol-1-yl)propylcarbamoyl)piperidine-1-carboxylate (8)	This study	N/A
4-amino-N-(3-(4-((4-(2-(4-chlorophenoxy)ethyl)piperazin-1-yl)methyl)-3-(3-fluorophenyl)-1H-indol-1-yl)propyl)piperidine-4-carboxamide: 3443	This study	N/A
5-chloro-2-(4-(trifluoromethoxy)benzyloxy)benzaldehyde	This study	N/A
4-((5-chloro-2-((4-(trifluoromethoxy)benzyl)oxy)benzyl)amino)-N-(3-(4-((4-(2-(4-chlorophenoxy)ethyl)piperazin-1-yl)methyl)-3-(3-fluorophenyl)-1H-indol-1-yl)propyl)piperidine-4-carboxamide (3495)	This study	N/A
N-(3-(5-((4-(3,5-dimethoxybenzyl)piperazin-1-yl)methyl)-3-(2,4-dimethoxyphenyl)-1H-indol-1-yl)propyl)piperazine-2-carboxamide (3603)	This study	N/A
4-amino-N-(3-(4-((4-(2-(4-chlorophenoxy)ethyl)piperazin-1-yl)methyl)-3-(2-methoxyphenyl)-1H-indol-1-yl)propyl)piperidine-4-carboxamide (3445)	This study	N/A
N-(3-(5-((4-(3,5-bis(trifluoromethyl)benzyl)piperazin-1-yl)methyl)-3-(2,6-bis(trifluoromethyl)phenyl)-1H-indol-1-yl)propyl)piperazine-2-carboxamide (3256)	This study	N/A
N-(3-(5-((4-(2,6-dichlorobenzyl)piperazin-1-yl)methyl)-3-(4-(trifluoromethoxy)phenyl)-1H-indol-1-yl)propyl)-4-((4-((3,5-dimethoxybenzyl)oxy)-3-methoxybenzyl)amino)piperidine-4-carboxamide (4363)	This study	N/A
4-((3-chloro-4-((4-fluorobenzyl)oxy)benzyl)amino)-N-(3-(4-((4-(2-(4-chlorophenoxy)ethyl)piperazin-1-yl)methyl)-3-(3-fluorophenyl)-1H-indol-1-yl)propyl)piperidine-4-carboxamide (3512)	This study	N/A
4-((4-((3,5-bis(trifluoromethyl)benzyl)oxy)benzyl)amino)-N-(3-(5-((4-(2,6-dichlorobenzyl)piperazin-1-yl)methyl)-3-(4-(trifluoromethoxy)phenyl)-1H-indol-1-yl)propyl)piperidine-4-carboxamide (4365)	This study	N/A
N-(3-(5-((4-(2,6-dichlorobenzyl)piperazin-1-yl)methyl)-3-(4-(trifluoromethoxy)phenyl)-1H-indol-1-yl)propyl)-4-(((5-(2-isopropoxyphenyl)pyridin-2-yl)methyl)amino)piperidine-4-carboxamide (4373)	This study	N/A
Critical Commercial Assays		
Lipofectamine 2000	ThermoFisher Scientific	Cat. No. 11668019
Lipofectamine RNAiMAX Transfection Reagent	Life Technologies	Cat. No. 13778-150
Mouse microsomes (CD-1)	Life Technologies	Cat. No. MSMCPL
Human microsomes (pooled 50 donors, 20 mg/mL)	ThermoFisher Scientific	Cat. No. HMMCPL
QIAshredder	Qiagen	Cat. No. 79656
RNAeasy extraction kit	Qiagen	Cat. No. 74106
TaqMan Reverse Transcription Reagents	Applied Biosystems	Cat. No. N8080234
Power SYBR Green PCR Master Mix	Thermo Fisher Scientific	Cat. No. 4368702
ImmPACT DAB Peroxidase Substrate Kit	Vector Labs	Cat. No. SK-4105

REAGENT or RESOURCE	SOURCE	IDENTIFIER
ImmPRESS HRP Anti-Rabbit IgG Peroxidase Polymer Detection Kit	Vector Labs	Cat. No. MP-7401
CellTiter-Glo Luminescent Cell Viability Assay	Promega	Cat. No. G7573
Apo-One Caspase 3/7 assay	Promega	Cat. No. G7790
Deposited Data		
Raw mass spectrometry files https://chorusproject.org/anonymous/download/experiment/3708034170230406717	This paper	https://chorusproject.org/
Experimental Models: Cell Lines		
Phoenix-AMPHO	ATCC	Cat. No. CRL-3213
Kras$^{lox/lox}$, *Hras*$^{-/-}$, *Nras*$^{-/-}$ *RERTn*$^{ert/ert}$ mouse embryo fibroblasts (MEFs)	Laboratory of Mariano Barbacid	Cat. No. DU315-6
Hras$^{-/-}$; *Nras*$^{-/-}$; *Kras*$^{lox/lox}$ BRAF(V600E)-^{CAAX} MEFs	This paper	N/A
DLD-1	ATCC	Cat. No. CCL-221
BL21-Gold (DE3) Competent Cells	Stratagene	Cat. No. 230132
MDA-MB-231	ATCC	Cat. No. HTB-26
Experimental Models: Organisms/Strains		
C57 male Mus musculus (mouse), 6–7 weeks of age, ~25g weight, black coat color, MHC Haplotype H2b	Charles River Laboratories	Strain: 027 (C57BL/6)
Nu/Nu athymic nude *Mus musculus* (mouse), Crl:NU-Foxn1nu, hairless, albino	Charles River Laboratories	Strain:088 (Homozygous)
KRAS^{LSLG12D}; p53$^{fl/fl}$; Pdx1-Cre (KP$^{f/f}$C) mice	Laboratory of Ken Olive	N/A
Mus musculus (mouse), Strain: Rag2-γc-, female, 4 weeks old, weight 22–24g, Genotype:Il2rg$^{tm1.1Flv}$ Rag2$^{tm1.1Flv}$	Jackson Laboratories	Cat. No. 014593 | Rag2-γc-
Recombinant DNA		
BRAF(V600E)^{CAAX} plasmid	This paper	N/A
pBABE-puro plasmid	Addgene	Plasmid # 1764
pBABE puro KRAS G12V	Addgene	Plasmid # 9052
pBabe puro BRAF-V600E	Addgene	Plasmid # 15269
pBabe puro HA PIK3CA E545K	Addgene	Plasmid # 12525
pBABEbleo-Flag-BRAF V600E	Addgene	Plasmid # 53156
pLL7.0: Venus-iLID-CAAX plasmid	Addgene	Plasmid # 60411
Human *KRAS4B* sequence containing the oncogenic Q61H mutation in pENTR221 vector	Invitrogen	Ultimate ORF Clone IOH9852
Wild-type human *KRAS4B* sequence in pENTR221 vector	This study	N/A
G12D *KRAS4B* encoding the catalytic domain (amino acids 1-169) cloned into *Nde I-BamH I* sites of pET-15b vector (Novagen) containing N-terminal His_6 tag.	This study	N/A
Sequence-Based Reagents		
ON-TARGETplus siRNA SMARTpool targeting HRAS	GE Dharmacon	Cat No. L-004142-00-0005
ON-TARGETplus siRNA SMARTpool targeting NRAS	GE Dharmacon	Cat No. L-003919-00-0005
ON-TARGETplus siRNA SMARTpool targeting KRAS	GE Dharmacon	Cat No. L-005069-00-0010
ON-TARGETplus Non-targeting Pool siRNAs	GE Dharmacon	Cat No. D-001810-10-20

REAGENT or RESOURCE	SOURCE	IDENTIFIER
siDEATH: AllStars Hs Cell Death Control siRNA	QIAGEN	Cat No. 1027299
Software and Algorithms		
Glide version 2012–2016 (Schrödinger Suite)	Schrödinger, Inc.	N/A
Molecular Operating Environment	Chemical Computing Group	N/A
ChemDraw Ultra	Perkin Elmer	version 10.0
Prism 5.0c	GraphPad Software	N/A
Other		
PrestoBlue Cell Viability Reagent	Life Technologies	Cat. No. A13262
Fetal Bovine Serum	Thermo Fisher Scientific	Cat. No. 10437-028
Heat inactivated fetal bovine serum		
Penicillin-Streptomycin, liquid	Thermo Fisher Scientific	Cat. No. 15140163
Dulbecco's Modified Eagle Medium	Fisher Scientific	Cat. No. 10-013-CM
Opti-mem	Invitrogen	
Polybrene	Santa Cruz Biotechnology	Cat. No. sc-134220
1X RPMI 1640 vitamin stock	Sigma-Aldrich	Cat. No. R7256
GlutaMAX	Life Technologies	Cat. No. 35050-061
CellTiter-Glo® Luminescent Cell Viability Assay	Promega	Cat. No. G7573
Corning Gentest 3P NADPH regenerating system solution A	Fisher Scientific	Cat. No. NC1096251
Corning Gentest 3P NADPH regenerating system system B	Fisher Scientific	Cat. No. NC1095811
QuikChange II Site-Directed Mutagenesis Kit, 10 Rxn	Agilent Technologies	Cat. No. 200523
Protease inhibitor tablet	Sigma-Aldrich	Cat. No. 11836170001
Ni Sepharose 6 Fast Flow beads	GE Life Sciences	Cat. No. 17-5318-01
NAP-5 Columns (GE Healthcare), 20 P	GE Life Sciences	Cat. No. 17-0853-01
Raf-1 RBD agarose beads	EMD Millipore	Cat. No. 14-278
Ral Assay Reagent (Ral BP1, agarose)	EMD Millipore	Cat. No. 14-415
Protein Labeling Kit RED-MALEIMIDE Monolith NT.115 (Cysteine Reactive)	NanoTemper Technologies GmbH	Cat. No. MO-L004
Standard Treated Capillaries Monolith NT.115	NanoTemper Technologies GmbH	Cat. No. MO-K002
NT-647-NHS-ester dye	NanoTemper Technologies GmbH	Cat. No. MO-L001
SYPRO® Orange Protein Gel Stain (5,000X Concentrate in DMSO)	Thermo Fisher Scientific	Cat. No. S6650
250 UN alkaline phosphatase on agar beads	Sigma-Aldrich	Cat. No. P0762
Corningware Ultra Low Attachment (ULA) Plates	Corning	Cat. No. CLS 3474

Supplementary Material

Refer to Web version on PubMed Central for supplementary material.

Acknowledgments

We thank Neil Whalen, Stuart Myers and Howard Robinson for setting up the X29 beamline at the NSLS. The in-house X-ray diffraction instrument was purchased with an NIH grant to L.T. (S10OD012018). This research was supported by grants to BRS (NIH 5R01CA097061, 5R01GM085081, and R01CA161061). We thank Dr. John Decatur and the Columbia Chemistry NMR core facility (NSF grant CHE 0840451 and NIH grant 1S10RR025431-01A1) for assistance in compound characterization, Michael Gaschler for providing the RHEB protein used for microscale thermophoresis, Dr. Michael Goger from New York Structural Biology Center (NYSBC) for assistance with 3D-NMR data acquisition. We thank Neil Whalen, Stuart Myers and Howard Robinson for setting up the X29 beamline at the NSLS. The in-house X-ray diffraction instrument was purchased with an NIH grant to LT (S10OD012018). B.R.S. is a member of the New York Structural Biology Center. The data collected at NYSBC was made possible by a grant from NYSTAR. AK was supported by the Training Program in Molecular Biophysics T32GM008281. BRS is a founder, consultant and shareholder of Kyras Therapeutics, which has licensed intellectual property described in this manuscript; BRS and MEW are recipients of royalty payments from this license. All animal studies were approved by the Columbia University IACUC.

References

Adams PD, Grosse-Kunstleve RW, Hung L-W, Ioerger TR, McCoy AJ, Moriarty NW, Read RJ, Sacchettini JC, Sauter NK, Terwilliger TC. PHENIX: building a new software for automated crystallographic structure determination. Acta Cryst. 2002; D58:1948–1954.

Arkin MR, Tang Y, Wells JA. Small-molecule inhibitors of protein-protein interactions: progressing toward the reality. Chem Biol. 2014; 21:1102–1114. [PubMed: 25237857]

Arkin MR, Wells JA. Small-molecule inhibitors of protein-protein interactions: progressing towards the dream. Nat Rev Drug Discov. 2004; 3:301–317. [PubMed: 15060526]

Bardeesy N, Aguirre AJ, Chu GC, Cheng KH, Lopez LV, Hezel AF, Feng B, Brennan C, Weissleder R, Mahmood U, et al. Both p16(Ink4a) and the p19(Arf)-p53 pathway constrain progression of pancreatic adenocarcinoma in the mouse. Proc Natl Acad Sci USA. 2006; 103:5947–5952. [PubMed: 16585505]

Block C, Janknecht R, Herrmann C, Nassar N, Wittinghofer A. Quantitative structure-activity analysis correlating Ras/Raf interaction in vitro to Raf activation in vivo. Nature structural biology. 1996; 3:244–251. [PubMed: 8605626]

Burns MC, Sun Q, Daniels RN, Camper D, Kennedy JP, Phan J, Olejniczak ET, Lee T, Waterson AG, Rossanese OW, et al. Approach for targeting Ras with small molecules that activate SOS-mediated nucleotide exchange. Proc Natl Acad Sci USA. 2014; 111:3401–3406. [PubMed: 24550516]

Burris HA 3rd, Moore MJ, Andersen J, Green MR, Rothenberg ML, Modiano MR, Cripps MC, Portenoy RK, Storniolo AM, Tarassoff P, et al. Improvements in survival and clinical benefit with gemcitabine as first-line therapy for patients with advanced pancreas cancer: a randomized trial. J Clin Oncol. 1997; 15:2403–2413. [PubMed: 9196156]

Chiang MY, Xu L, Shestova O, Histen G, L'Heureux S, Romany C, Childs ME, Gimotty PA, Aster JC, Pear WS. Leukemia-associated NOTCH1 alleles are weak tumor initiators but accelerate K-ras-initiated leukemia. The Journal of clinical investigation. 2008; 118:3181–3194. [PubMed: 18677410]

Colletti LM, Liu Y, Koev G, Richardson PL, Chen CM, Kati W. Anal Biochem. 2008; 383(2):186. [PubMed: 18790690]

Colicelli J. Human RAS superfamily proteins and related GTPases. Sci STKE. 2004; 2004:RE13. [PubMed: 15367757]

Cox AD, Fesik SW, Kimmelman AC, Luo J, Der CJ. Drugging the undruggable RAS: Mission possible? Nat Rev Drug Discov. 2014; 13:828–851. [PubMed: 25323927]

Dolma S, Lessnick SL, Hahn WC, Stockwell BR. Identification of genotype-selective antitumor agents using synthetic lethal chemical screening in engineered human tumor cells. Cancer Cell. 2003; 3:285–296. [PubMed: 12676586]

Downward J. Targeting RAS signalling pathways in cancer therapy. Nat Rev Cancer. 2003; 3:11–22. [PubMed: 12509763]

Geoghegan KF, Dixon HBF, Rosner PJ, Hoth LR, Lanzetti AJ, Borzilleri KA, Marr ES, Pezzullo LH, Martin LB, LeMotte PK, et al. Spontaneous alpha-N-6-phosphogluconoylation of a “His tag” in Escherichia coli: The cause of extra mass of 258 or 178 Da in fusion proteins. Analytical Biochemistry. 1999; 267:169–184. [PubMed: 9918669]

Gysin S, Salt M, Young A, McCormick F. Therapeutic strategies for targeting ras proteins. Genes & cancer. 2011; 2:359–372. [PubMed: 21779505]

Hall BE, Bar-Sagi D, Nassar N. The structural basis for the transition from Ras-GTP to Ras-GDP. PNAS. 2002; 99:12138–12142. [PubMed: 12213964]

Hewitt SH, Wilson AJ. Metal complexes as “protein surface mimetics”. Chem Commun (Camb). 2016; 52:9745–9756. [PubMed: 27353704]

Hopkins AL, Groom CR. The druggable genome. Nat Rev Drug Discov. 2002; 1:727–730. [PubMed: 12209152]

Huang L, Hofer F, Martin GS, Kim SH. Structural basis for the interaction of Ras with RalGDS. Nature structural biology. 1998; 5:422–426. [PubMed: 9628477]

Huang L, Weng X, Hofer F, Martin GS, Kim SH. Three-dimensional structure of the Ras-interacting domain of RalGDS. Nature structural biology. 1997; 4:609–615. [PubMed: 9253406]

Jahnke, W., Erlanson, DA. Fragment-based approaches in drug discovery. Weinheim Chichester: Wiley-VCH ; John Wiley, distributor; 2006.

Johnson L, Greenbaum D, Cichowski K, Mercer K, Murphy E, Schmitt E, Bronson RT, Umanoff H, Edelmann W, Kucherlapati R, et al. K-ras is an essential gene in the mouse with partial functional overlap with N-ras. Genes Dev. 1997; 11:2468–2481. [PubMed: 9334313]

Kaelin WG Jr. The concept of synthetic lethality in the context of anticancer therapy. Nat Rev Cancer. 2005; 5:689–698. [PubMed: 16110319]

Karnoub AE, Weinberg RA. Ras oncogenes: split personalities. Nat Rev Mol Cell Biol. 2008; 9:517–531. [PubMed: 18568040]

Malumbres M, Barbacid M. RAS oncogenes: the first 30 years. Nat Rev Cancer. 2003; 3:459–465. [PubMed: 12778136]

Maurer T, Garrenton LS, Oh A, Pitts K, Anderson DJ, Skelton NJ, Fauber BP, Pan B, Malek S, Stokoe D, et al. Small-molecule ligands bind to a distinct pocket in Ras and inhibit SOS-mediated nucleotide exchange activity. Proc Natl Acad Sci USA. 2012; 109:5299–5304. [PubMed: 22431598]

McCormick F. Cancer therapy based on oncogene addiction. J Surg Oncol. 2011; 103:464–467. [PubMed: 21480237]

McCoy AJ, Grosse-Kunstleve RW, Adams PD, Winn MD, Storoni LC, Read RJ. Phaser crystallographic software. J Appl Cryst. 2007; 40:658–674. [PubMed: 19461840]

Murshudov GN, Vagin AA, Dodson EJ. Refinement of macromolecular structures by the maximum-likelihood method. Acta Cryst. 1997; D53:240–255.

Oberstein PE, Olive KP. Pancreatic cancer: why is it so hard to treat? Therap Adv Gastroenterol. 2013; 6:321–337.

Ostrem JM, Peters U, Sos ML, Wells JA, Shokat KM. K-Ras(G12C) inhibitors allosterically control GTP affinity and effector interactions. Nature. 2013; 503:548–551. [PubMed: 24256730]

Ostrem JM, Shokat KM. Direct small-molecule inhibitors of KRAS: from structural insights to mechanism-based design. Nat Rev Drug Discov. 2016

Otwinowski Z, Minor W. Processing of X-ray diffraction data collected in oscillation mode. Method Enzymol. 1997; 276:307–326.

Pacold ME, Suire S, Perisic O, Lara-Gonzalez S, Davis CT, Walker EH, Hawkins PT, Stephens L, Eccleston JF, Williams RL. Crystal structure and functional analysis of Ras binding to its effector phosphoinositide 3-kinase gamma. Cell. 2000; 103:931–943. [PubMed: 11136978]

Piovan E, Yu J, Tosello V, Herranz D, Ambesi-Impiombato A, Da Silva AC, Sanchez-Martin M, Perez-Garcia A, Rigo I, Castillo M, et al. Direct reversal of glucocorticoid resistance by AKT inhibition in acute lymphoblastic leukemia. Cancer cell. 2013; 24:766–776. [PubMed: 24291004]

Prior IA, Hancock JF. Ras trafficking, localization and compartmentalized signalling. Seminars in cell & developmental biology. 2012; 23:145–153. [PubMed: 21924373]

Prior IA, Lewis PD, Mattos C. A comprehensive survey of ras mutations in cancer. Cancer Res. 2012; 72:2457–2467. [PubMed: 22589270]

Sastra SA, Olive KP. Acquisition of Mouse Tumor Biopsies through Abdominal Laparotomy. Cold Spring Harb Protoc. Jan 1.2014 (1):47–56. [PubMed: 24371318]

Scheffzek K, Ahmadian MR, Kabsch W, Wiesmuller L, Lautwein A, Schmitz F, Wittinghofer A. The Ras-RasGAP complex: structural basis for GTPase activation and its loss in oncogenic Ras mutants. Science. 1997; 277:333–338. [PubMed: 9219684]

Shaw RJ, Cantley LC. Ras, PI(3)K and mTOR signalling controls tumour cell growth. Nature. 2006; 441:424–430. [PubMed: 16724053]

Shima F, Yoshikawa Y, Ye M, Araki M, Matsumoto S, Liao J, Hu L, Sugimoto T, Ijiri Y, Takeda A, et al. In silico discovery of small-molecule Ras inhibitors that display antitumor activity by blocking the Ras-effector interaction. Proc Natl Acad Sci USA. 2013; 110:8182–8187. [PubMed: 23630290]

Spiegel J, Cromm PM, Zimmermann G, Grossmann TN, Waldmann H. Small-molecule modulation of Ras signaling. Nat Chem Biol. 2014; 10:613–622. [PubMed: 24929527]

Stephen AG, Esposito D, Bagni RK, McCormick F. Dragging ras back in the ring. Cancer Cell. 2014; 25:272–281. [PubMed: 24651010]

Sun Q, Burke JP, Phan J, Burns MC, Olejniczak ET, Waterson AG, Lee T, Rossanese OW, Fesik SW. Discovery of small molecules that bind to K-Ras and inhibit Sos-mediated activation. Angew Chem Int Ed Engl. 2012; 51:6140–6143. [PubMed: 22566140]

Sun Q, Phan J, Friberg AR, Camper DV, Olejniczak ET, Fesik SW. A method for the second-site screening of K-Ras in the presence of a covalently attached first-site ligand. J Biomol NMR. 2014; 60:11–14. [PubMed: 25087006]

Tanaka T, Rabbitts TH. Interfering with RAS-effector protein interactions prevent RAS-dependent tumour initiation and causes stop-start control of cancer growth. Onco. 2010; 29:6064–6070.

Tsutsumi K, Fujioka Y, Tsuda M, Kawaguchi H, Ohba Y. Visualization of Ras-PI3K interaction in the endosome using BiFC. Cell Signal. 2009; 21:1672–1679. [PubMed: 19616621]

Urosevic J, Sum EY, Moneo V, Drosten M, Dhawahir A, Becerra M, Carnero A, Barbacid M. Using cells devoid of RAS proteins as tools for drug discovery. Mol Carcinog. 2009; 48:1038–1047. [PubMed: 19526460]

van Hattum H, Waldmann H. Chemical biology tools for regulating RAS signaling complexity in space and time. Chem Biol. 2014; 21:1185–1195. [PubMed: 25237862]

Vassilev LT, Vu BT, Graves B, Carvajal D, Podlaski F, Filipovic Z, Kong N, Kammlott U, Lukacs C, Klein C, et al. In vivo activation of the p53 pathway by small-molecule antagonists of MDM2. Science. 2004; 303:844–848. [PubMed: 14704432]

Vigil D, Cherfils J, Rossman KL, Der CJ. Ras superfamily GEFs and GAPs: validated and tractable targets for cancer therapy? Nature reviews Cancer. 2010; 10:842–857. [PubMed: 21102635]

Vo U, Embrey KJ, Breeze AL, Golovanov AP. 1H, 13C and 15N resonance assignment for the human K-Ras at physiological pH. Biomol NMR Assign. 2013; 7:215–219. [PubMed: 22886485]

Walker K, Olson MF. Targeting Ras and Rho GTPases as opportunities for cancer therapeutics. Curr Opin Genet Dev. 2005; 15:62–68. [PubMed: 15661535]

Wang W, Fang G, Rudolph J. Ras inhibition via direct Ras binding--is there a path forward? Bioorg Med Chem Lett. 2012; 22:5766–5776. [PubMed: 22902659]

Ward AF, Braun BS, Shannon KM. Targeting oncogenic Ras signaling in hematologic malignancies. Blood. 2012; 120:3397–3406. [PubMed: 22898602]

Weiwer M, Bittker JA, Lewis TA, Shimada K, Yang WS, MacPherson L, Dandapani S, Palmer M, Stockwell BR, Schreiber SL, et al. Development of small-molecule probes that selectively kill cells induced to express mutant RAS. Bioorg Med Chem Lett. 2012; 22:1822–1826. [PubMed: 22297109]

Yang WS, Stockwell BR. Synthetic lethal screening identifies compounds activating iron-dependent, nonapoptotic cell death in oncogenic-RAS-harboring cancer cells. Chem Biol. 2008; 15:234–245. [PubMed: 18355723]

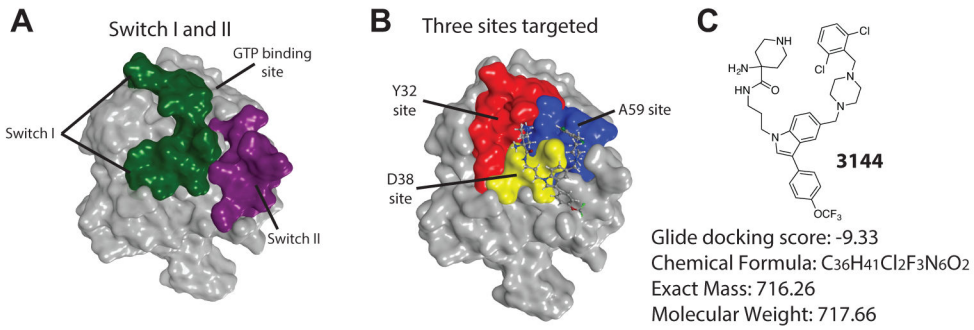

Figure 1. Design of inhibitor of RAS proteins

(A) $KRAS^{G12D}$ (PDB: 4DSN) with the switch I region shown in green and the switch 2 region in purple. **(B)** Location of three sites on $KRAS^{G12D}$ targeted (D38 site in yellow, A59 site in blue, Y32 site in red), with pose of docked 3144 ligand. **(C)** Structure, docking score, chemical formula, mass and molecular weight of the small molecule 3144. See also Figure S1, Table S1 and Supporting Information.

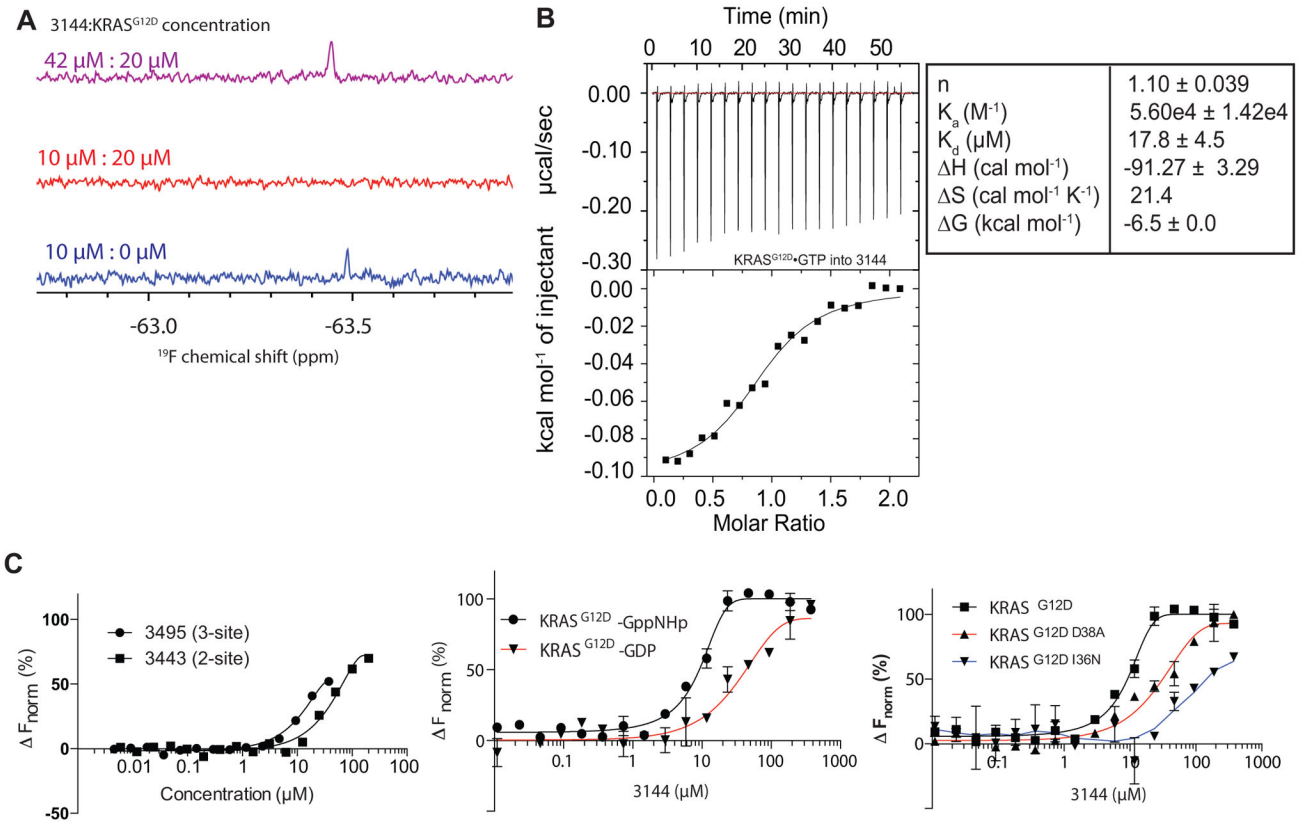

D

Protein	3144 K_D (µM)
KRAS^{G12D}-GppNHp	4.7 ± 0.4
KRAS(wt)-GppNHp	17 ± 6
HRAS-GppNHp	6.6 ± 0.8
NRAS-GppNHp	3.7 ± 0.6
RRAS2-GppNHp	24 ± 32
RRAS-GppNHp	no binding
RAP1A-GppNHp	no binding
RHEB-GppNHp	no binding
RHOA-GppNHp	no binding
RALA-GppNHp	no binding

E

Protein	3144 K_D (µM)
KRAS^{G12D}-GppNHp	6.2 ± 0.5
KRAS$^{G12D, I36N}$-GppNHp	33 ± 0.6
KRAS$^{G12D, D38A}$-GppNHp	44 ± 6

F

Protein	Nucleotide	Tm (°C)
KRAS^{G12D}	endogenous	51.2 ± 0.1
KRAS^{G12D}	GTP	49.3 ± 0.8
KRAS$^{G12D\ I36N}$	endogenous	49.8 ± 0.3
KRAS$^{G12D\ I36N}$	GTP	47.8 ± 0.1
KRAS$^{G12D\ D38A}$	endogenous	57.7 ± 0.4
KRAS$^{G12D\ D38A}$	GTP	55.2 ± 0.3

Figure 2. 3144 binds to KRAS^{G12D}

(A) ^{19}F NMR spectrum of 3144 titrated into KRAS^{G12D} (GppNHp-bound) at the indicated concentrations. **(B)** ITC binding assay with 3144 and KRAS^{G12D}-GppNHp. **(C)** (left panel) MST assay of the three-site compound 3495 and the two-site compound from which it was derived, 3443, using KRAS^{G12D}-GppNHp, (middle panel) MST assay with 3144 and its differential selectivity towards GppNHp-bound vs. GDP-bound KRAS^{G12D}**,** and (right panel) MST assay with two different point mutants within the predicted docking site on KRAS^{G12D}-GppNHp and 3144. **(D and E)** Summary of K_D values obtained for binding of 3144 to the indicated proteins by MST. **(F)** Melting temperatures of the indicated proteins with either endogenous nucleotide or GTP (after nucleotide exchange); the shift in melting temperature indicates successful exchange of bound nucleotide. See also Figure S2 and Supporting Information.

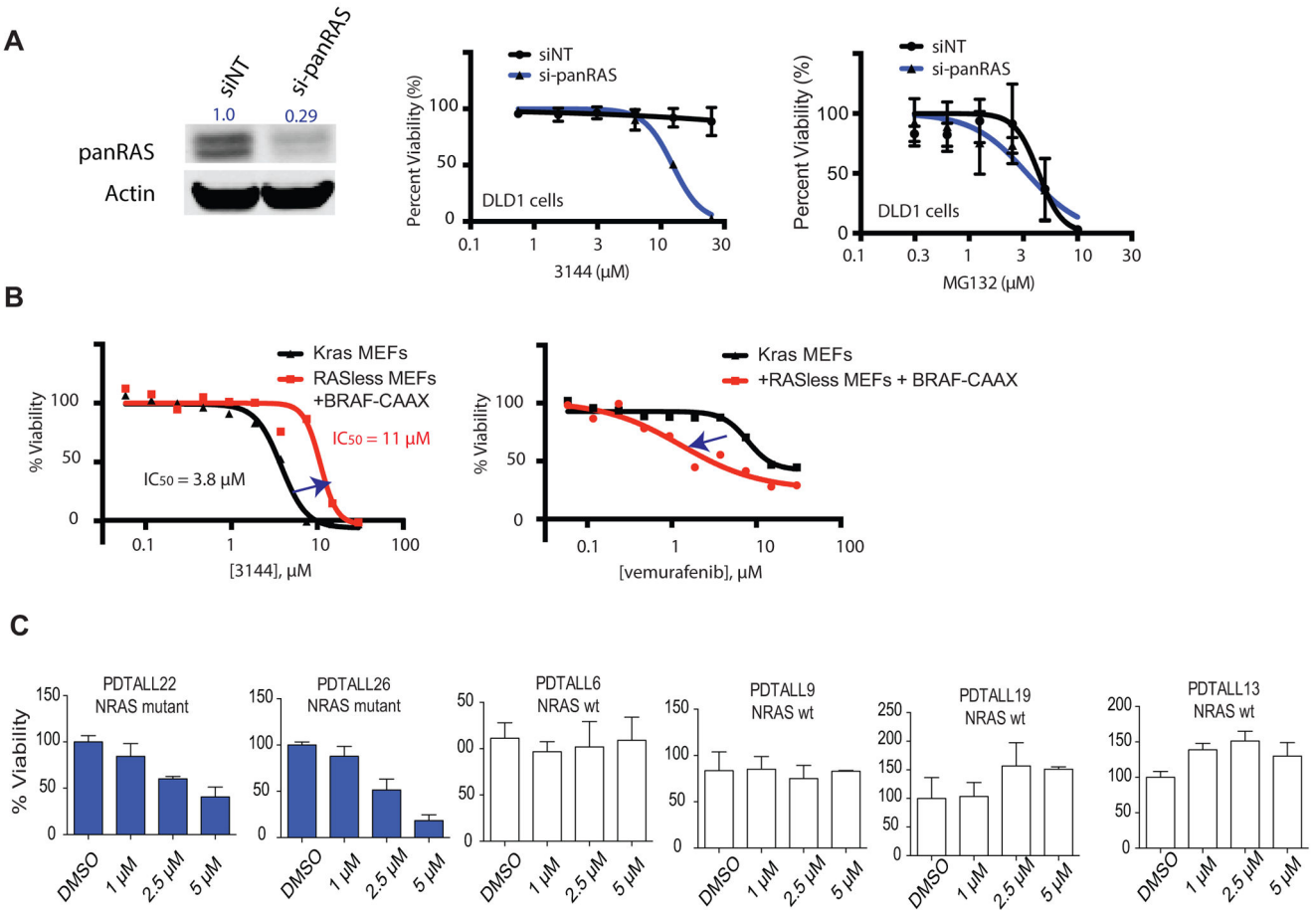

Figure 3. 3144 has RAS-dependent lethality

(A) (left panel) Inhibition of RAS expression in DLD-1 cells transfected with siRNAs targeting *HRAS*, *NRAS* and *KRAS (*si-panRAS) or a non-targeting siRNA control. Total Ras expression was determined with a pan-RAS antibody, as well as actin abundance. The total RAS abundance, normalized to actin abundance, is indicated. (middle and right panels) The concentration-dependent effects of 3144 and MG132 on DLD1 cells transfected with either si-panRAS or siNT was measured using Cell Titer Glo. (B) The effect of 3144 (left panel) and vemurafenib (right panel) on viability and growth of mouse embryo fibroblasts (MEFs) was measured at the indicated concentrations using Alamar blue. All compound measurements were performed in duplicate. Black line = $Kras^{lox/lox}$, $Hras^{-/-}$, $Nras^{-/-}$ $RERTn^{ert/ert}$ MEFs; red line = $BRAF^{V600E}$-CAAX; $Kras^{-/-}$, $Hras^{-/-}$, $Nras^{-/-}$ $RERTn^{ert/ert}$ MEFs. (C) The effect of 3144 was tested at the indicated concentrations in cultured patient-derived T-ALL samples. PDTALL6, 9, 13 and 19 = wt *NRAS*, PDTALL22 = $NRAS^{G13V}$, PDTALL26 = $NRAS^{G13D}$. See also Figure S3 and Supporting Information.

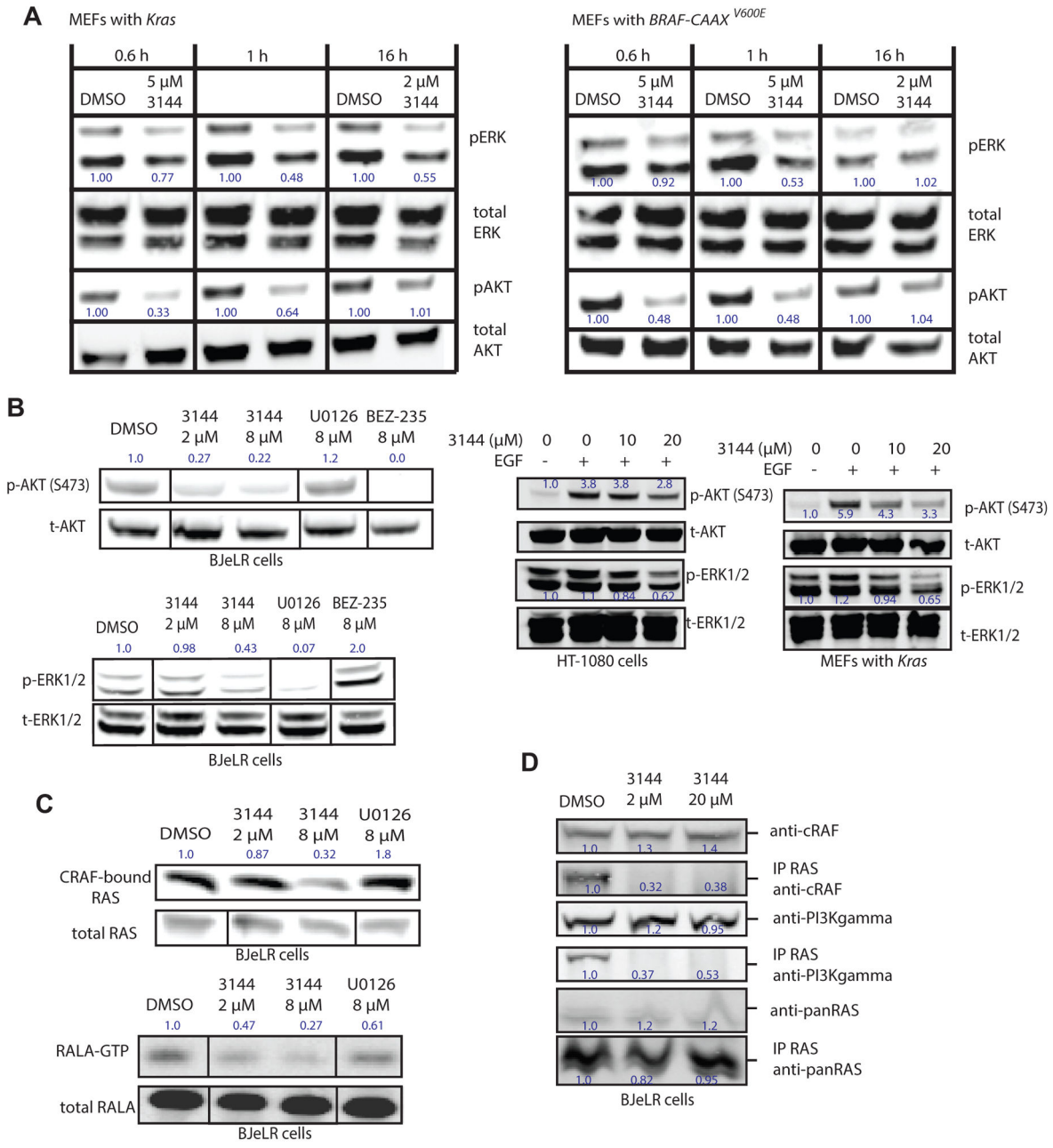

Figure 4. 3144 inhibits RAS-dependent signaling in cells

(A) 250,000 cells/well of the indicated MEFs were seeded in six-well dishes in medium with 10% FBS, then the next day the medium was changed to serum-free medium and the cells incubated for 24 h. 3144 or vehicle (DMSO) control were added the cells in serum-free medium for the indicated times. The cells were stimulated for 15 minutes with 10 ng/mL human EGF, then washed with cold PBS and analyzed by western blotting. The effects on abundance of phospho-ERK, total ERK, phospho-AKT, and total AKT were measured. The normalized relative abundance of pERK and pAKT is indicated next to these bands. (B) The effects of 3144, U0126 (MEK inhibitor) or BEZ-235 (PI3K inhibitor) on abundance of pAKT and total AKT (top left panel) and pERK and total ERK (bottom left panel) was

determined at the indicated concentrations in BJeLR engineered human tumor cells (with $HRAS^{V12}$). (right panel) A similar experiment was performed in HT-1080 cells and Kras MEFs: For HT-1080 cells, 1 million cells/well (6 well dishes) were seeded, and incubated overnight. The medium was replaced with serum free medium containing the indicated concentration of 3144. After 2 h, 10ng/mL EGF was added as indicated for 15 min. MEF cells were seeded at 700k cells/well in a 12 well plate, and incubated overnight. The following day, normal growth media was replaced with serum free media containing the indicated concentration of 3144. Cells were treated for 80 min, after which the medium was replaced with medium containing the indicated concentration of 3144 +/− EGF at 10 ng/mL as indicated. Cells were treated with EGF for 15 min. (C) (top panel) BJeLR cells were treated with 3144 or U0126 as indicated and the amount of c-RAF bound to RAS proteins was determined. The cells were then lysed and the lysate was incubated with CRAF RBD-agarose beads for 2 h before being washed 2× with PBS, denatured and subsequently detected by western blotting. (Bottom panel) Effect of 3144 on RAS-RALGDS pathway. BJeLR cells were seeded in 2% FBS in DMEM 18 h prior to treatment with 3144 and U0126 in 2% FBS in DMEM for 3 h. Cells were then lysed and the lysate was incubated with RalBP1 agarose beads for 2 h before being washed 2× with PBS, denatured and subsequently detected by western blotting. **(D)** BJeLR cells were seeded in 10% FBS in DMEM 18 hr prior to treatment with 3144 in 10% FBS in DMEM for 3 h, HRAS was immunoprecipitated and the indicated proteins examined for co-precipitation. The relative intensity of each band is indicated. See also Figure S4 and Supporting Information.

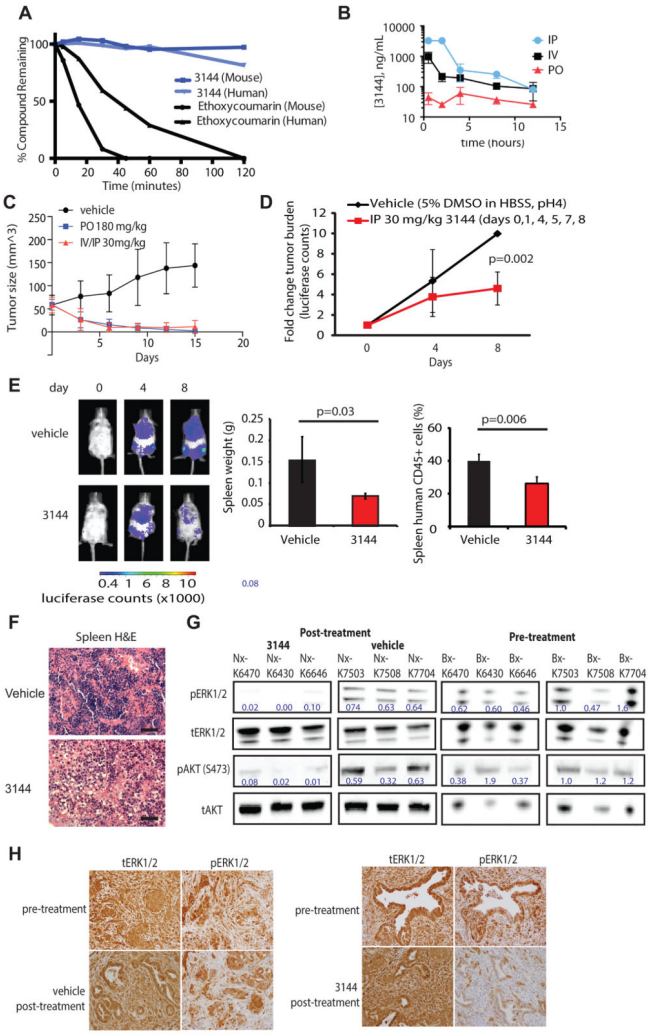

Figure 5. 3144 shows activity in a mutant RAS cell line xenograft and a patient-derived T-ALL xenograft

(A) Stability of 3144 in human liver microsomes: 3144 and 7-ethoxycoumarin were incubated for 120 min with mouse or human liver microsomes and the amount of compound remaining at each time point was quantified by LC-MS. **(B)** Pharmacokinetics of 3144: male C57BL6 adult mice were dosed orally or intravenously with 3144 in 10% NMP/90% PEG-400 at 30 mg/kg. Concentration in the plasma was measured over the course of 12 h. **(C)** Effect of 3144 in an MDA-MB-231 xenograft. Eight week old nude female mice were injected with 7 million MDA-MB-231 cells. After tumors reached an average size of 58 cubic millimeters they were treated with vehicle orally (10 doses), 3144 orally (180 mg/kg, 10 doses), or by a combination of intravenous and intraperitoneal injections (30 mg/kg, 4 IV doses, 6 IP doses) over two weeks. **(D)** Effect of 3144 on a patient-derived T-ALL sample PDTALL22 as a luciferase-expressing xenograft. Mice were randomized into two treatment groups of 5 mice with equal loads of luciferase. Mice were treated with 3144 (30 mg/kg) or vehicle intraperitoneal once daily on days: 0, 1, 4, 5, 7 and 8**. (E)** Representative images of mice from each treatment group at days, 0, 4 and 8 (final day) of the study in (D), and bar graph representing spleen weight in grams and percentage of human CD45+ cells in the

spleen of vehicle and 3144-treated mice. **(F)** Hematoxylin and eosin immunohistochemistry of spleen sections of mice treated with 3144 compared to vehicle. **(G)** Pre-treatment analysis (biopsy, Bx) and post-treatment analysis (necropsy, Nx) of tissue samples taken from $KP^{f/f}C$ mice by western blotting for phosphorylated ERK1/2, total ERK1/2, phosphorylated AKT (S473), and total AKT. Samples were taken prior to, or after five days of, treatment from each of three mice receiving either 3144 (30 mg/kg) or vehicle dosed once daily, intraperitoneally. **(H)** Analysis of phosphorylated ERK1/2 and total ERK1/2, detected by immunohistochemistry. Shown are images from representative sections of the biopsy and necropsy samples from 3144 and vehicle treated mice. See also Figure S5 and Supporting Information.